

Supporting Information

Morphological Control of $\text{Ca}_x\text{Mn}_{1-x}\text{Nb}_2\text{O}_6$ Columbites for Use as Lithium Hosts in Batteries

Wilgner Lima da Silva ^{a, e}, Marc Walker ^b, Rogério M. Ribas ^c, Robson S. Monteiro ^c, Emma Kendrick ^{d*}, Richard I. Walton ^{a*}

^a Department of Chemistry, University of Warwick, Gibbet Hill Road, Coventry CV4 7AL, United Kingdom

^b Department of Physics, University of Warwick, Gibbet Hill Road, Coventry CV4 7AL, United Kingdom

^c Companhia Brasileira de Metalurgia e Mineração (CBMM), Araxá, Minas Gerais 38183-903, Brazil

^d School of Metallurgy and Materials, University of Birmingham, Edgbaston, Birmingham B15 2TT, United Kingdom

^e WMG, University of Warwick, Gibbet Hill Road, Coventry CV4 7AL, United Kingdom

*Corresponding authors

E-mail addresses: e.kendrick@bham.ac.uk (E. Kendrick), r.i.walton@warwick.ac.uk (R. I. Walton)

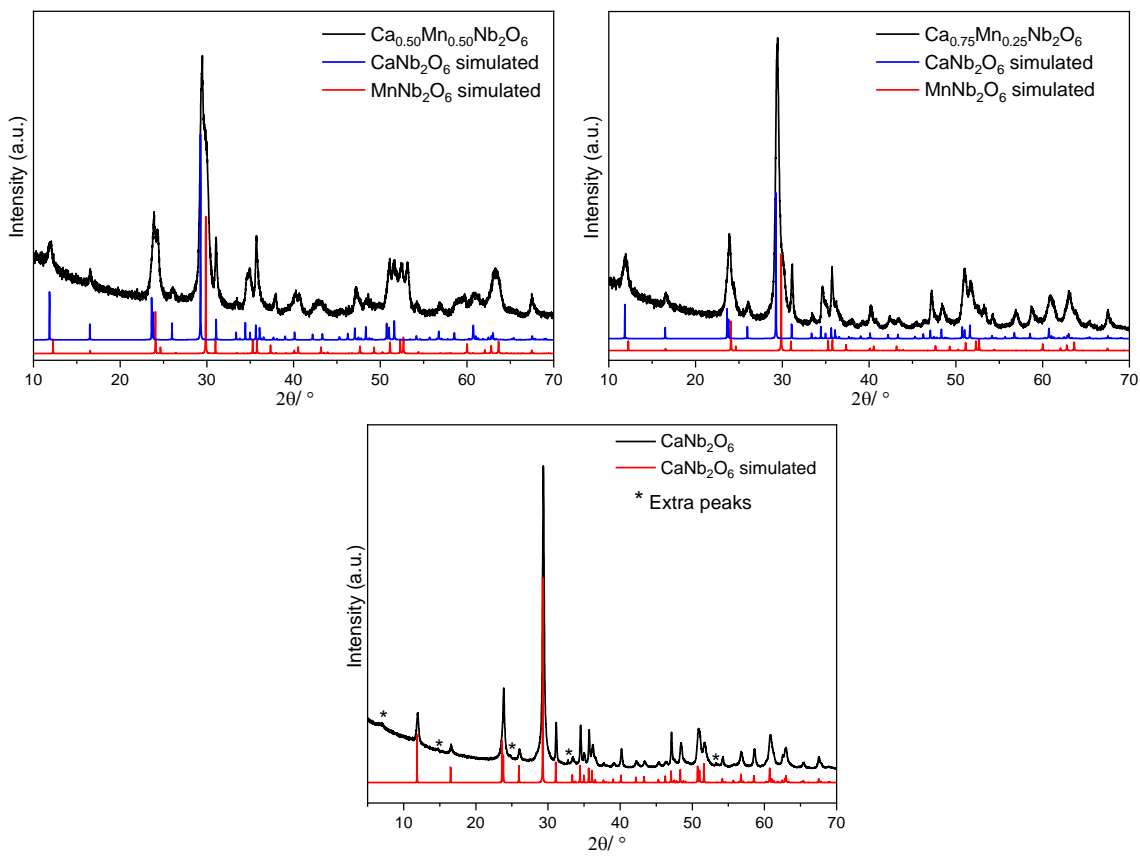


Figure S1: Attempted hydrothermal reactions to obtain $\text{Ca}_x\text{Mn}_{1-x}\text{Nb}_2\text{O}_6$ as $x > 0.25$. The PXRD shows that the introduction of higher percentage of Ca induces the formation of two phases. For the case of CaNb_2O_6 , it was observed the formation of another phase.

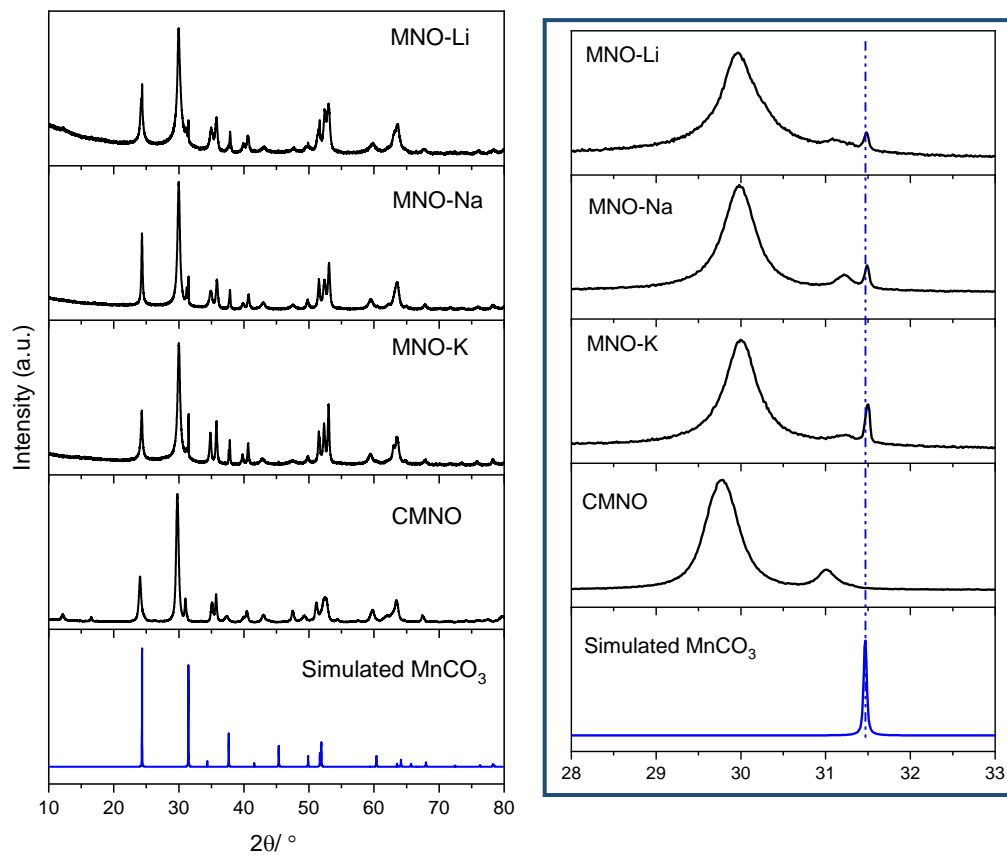


Figure S2: Powder X-ray diffraction patterns from the samples hydrothermally synthesised without purification (right), containing MnCO₃. CMNO does not appear to form carbonate as the Mn niobates, but the sample was once washed with acidic solution. Insert (right) depicts the diffracted peak from MnCO₃.

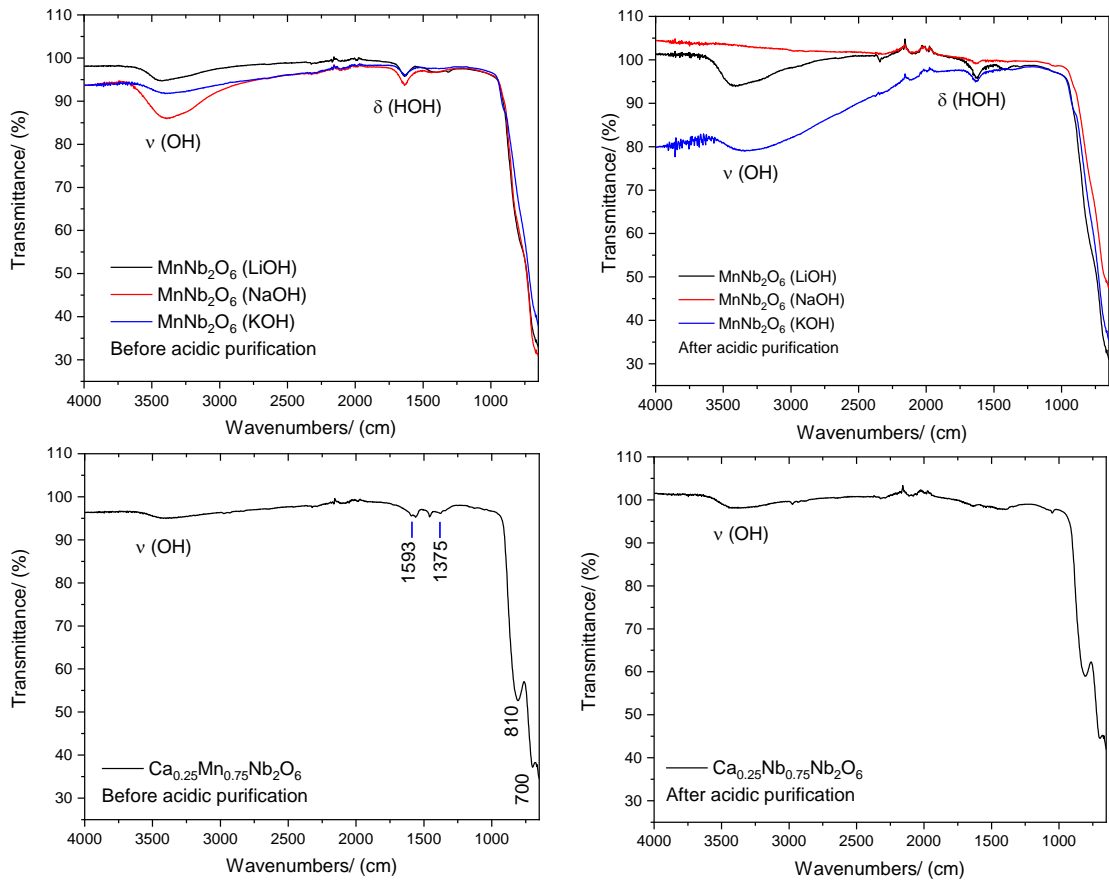


Figure S3: FT-IR spectra from MNO-Li, MNO-Na, and MNO-K (top) and CMNO (bottom) before and acetic acid treatment, respectively.

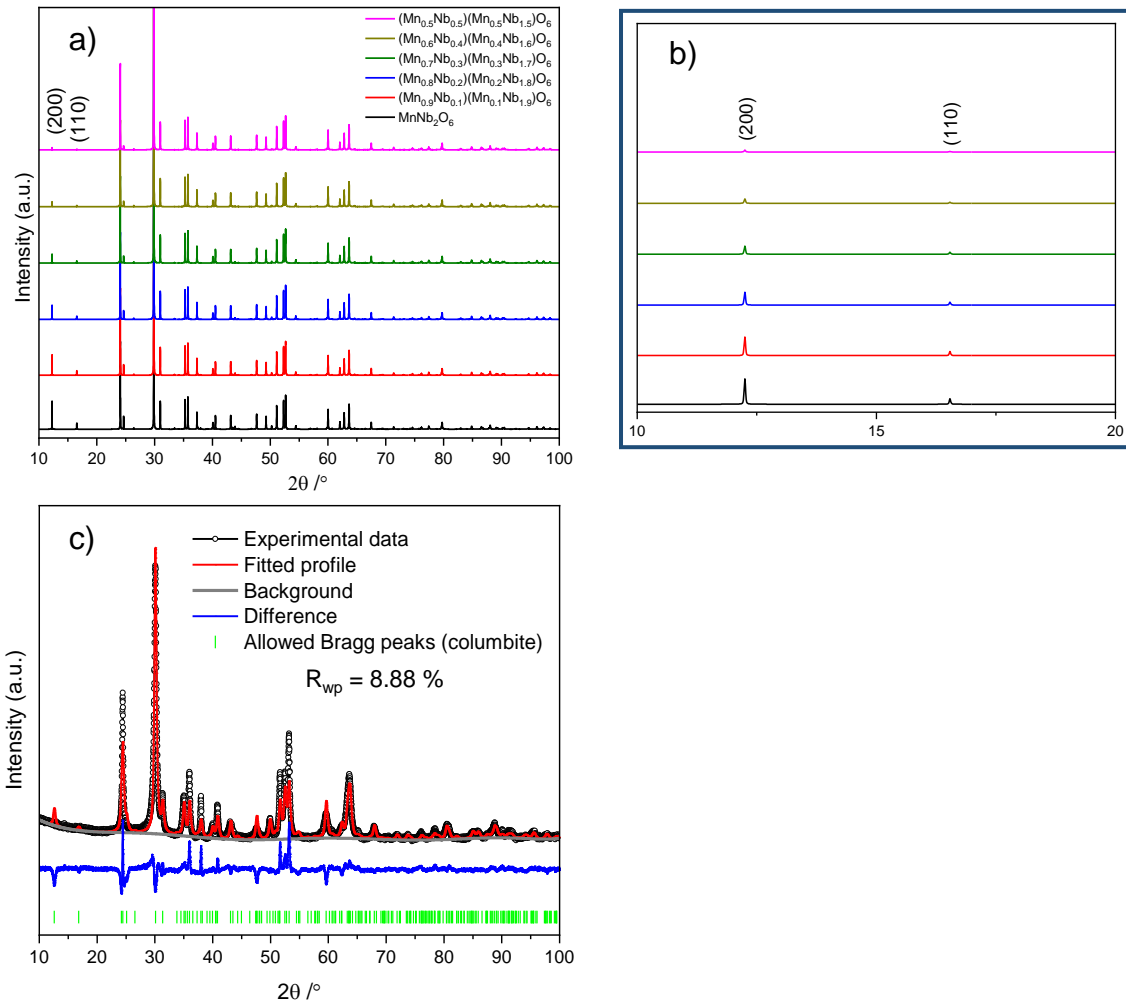


Figure S4: a) Simulated PXRD by intermixing Nb and Mn sites in MnNb₂O₆, illustrating that the only difference is the relative intensity of the peaks (200) and (110) using VESTA,¹ b) insert depicts the low angle region, and c) attempted Rietveld refinement using MnNb₂O₆ as the model (orthorhombic unit cell) ($\lambda = 1.54056 \text{ \AA}$).

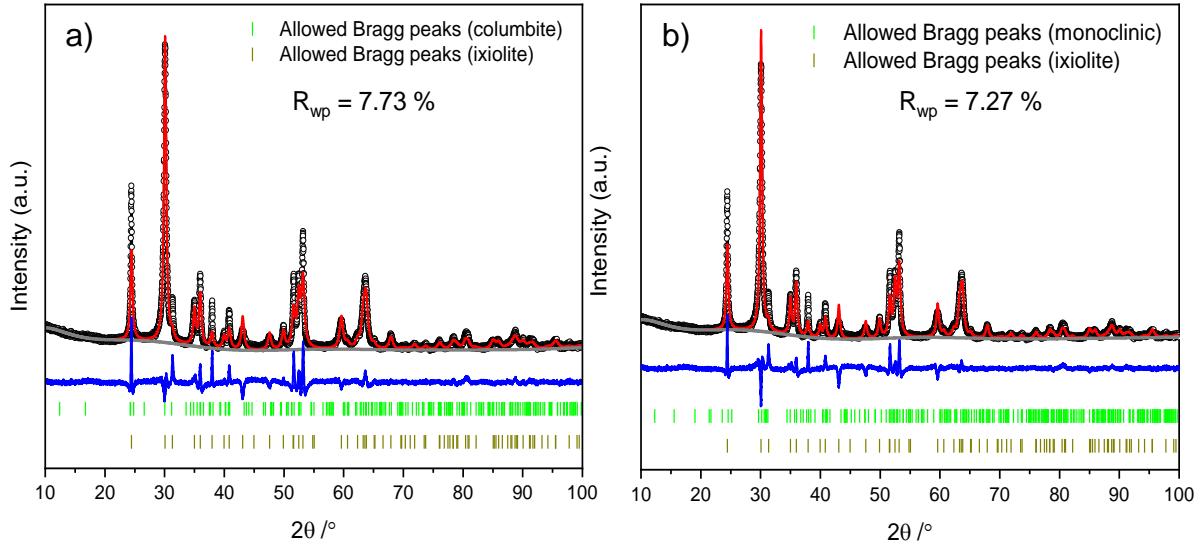


Figure S5: Rietveld refinement using two-unit cells a) columbite and ixiolite, and b) monoclinic and ixiolite using MNO-Na PXRD data. The monoclinic model can be discarded due to the main reflections are distinct from the PXRD profile. The presence of OH⁻ or H₂O in the structure cavities is not possible due to the low mass loss present in the TGA, which is not significant to be considered in the Rietveld refinement ($\lambda = 1.54056 \text{ \AA}$).

Table S1: Structural parameters obtained from Rietveld refinement against PXRD data from as-made MNO-Na using different unit cells. Attention must be made to the phase fraction converging to an ixiolite unit cell.

MnNb₂O₆ (NaOH) (as made)

Columbite

$R_{wp} = 8.88\%$, GOF = 3.47, $a = 14.284(1) \text{ \AA}$, $b = 5.7382(4) \text{ \AA}$, $c = 5.1479(4) \text{ \AA}$, Vol = 421.94(4) \AA^3 , $\rho = 5.3010 \text{ g}\cdot\text{cm}^{-3}$.

MnNb₂O₆ (NaOH) (as made)

Columbite

Phase fraction: 1×10^{-12}

Ixiolite

Phase fraction: 1.0

$R_{wp} = 7.73\%$, GOF = 2.97, $a = 4.7604(4) \text{ \AA}$, $b = 5.7386(5) \text{ \AA}$, $c = 5.1464(4) \text{ \AA}$, Vol = 140.588(11) \AA^3 , $\rho = 5.1920 \text{ g}\cdot\text{cm}^{-3}$.

MnNb₂O₆ (NaOH) (as made)

Monoclinic

Phase fraction: 1×10^{-12}

Ixiolite

Phase fraction: 1.0

$R_{wp} = 7.27\%$, GOF = 2.80, $a = 4.7607(3) \text{ \AA}$, $b = 5.7386(4) \text{ \AA}$, $c = 5.1468(3) \text{ \AA}$, Vol = 141.610(9) \AA^3 , $\rho = 5.3182 \text{ g}\cdot\text{cm}^{-3}$.

LiTa₃O₈ monoclinic (previously reported²)

Space group C2c

$a = 9.413(5) \text{ \AA}$, $b = 11.522(6) \text{ \AA}$, $c = 5.050(3) \text{ \AA}$, Vol = 547.61 \AA^3 , $\alpha = \gamma = 90^\circ$, $\beta = 91.50(10)^\circ$, $\rho = 8.22 \text{ g}\cdot\text{cm}^{-3}$.

Collection code ICSD 493

Rietveld refinement strategy – as-synthesised and sintered samples:

The Rietveld refinement strategy consisted of allowing the occupancies to refine, if they did not diverge far from one, they were set as one. The isotropic temperature factors (U_{iso}), used to describe the thermal parameters/behaviour of the atoms, were refined starting with heavier elements as Nb and Mn, and then O. Some of the values for the oxide ions became unphysical, once negative, probably because of the weak scattering power of light atoms using conventional laboratory X-ray diffraction. To solve it, the values for fewer oxygens were set to be positive and the refinement proceeded.

For the sintered samples, the same strategy was followed. In the case of sintered MNO-Li, refining the fraction sites suggests that the sample is Nb deficient after annealing, which agrees with having Nb_2O_5 as a minor impurity. Due to peak anisotropy, the anisotropic U values, U_{11} , U_{22} , U_{33} , U_{12} , U_{13} , U_{23} , were refined and gave a better fit. Nb_2O_5 only had its unit cells parameters refined. U_{iso} , occupancy and atomic position were not refined, Table S2.

MNO-Na has a slight amount of impurity, which could not be indexed to any existing phase. As shown in the Table S3, the main diffraction peaks for the unknown phase were added to the background.

Table S2: Nb_2O_5 unit cell parameters obtained from the Rietveld refinement against MNO-Li PXRD.

MnNb₂O₆ (LiOH) (sintered)

Nb_2O_5

Space group $P\bar{2}/m$

$a = 21.178(1)$ Å, $b = 3.8231(3)$ Å, $c = 19.37(1)$ Å, Vol = 1359.5 (2) Å³, $\alpha = \gamma = 90^\circ$, $\beta = 119.89(2)^\circ$, $\rho = 4.5453$ g·cm⁻³. Phase fraction: 0.0091349.

Nb₂O₅ (previously reported³)

$a = 21.153(7)$ Å, $b = 3.8233(5)$ Å, $c = 19.356(5)$ Å, Vol = 1358.40 Å³, $\alpha = \gamma = 90^\circ$, $\beta = 119.80(2)^\circ$, $\rho = 4.548$ g·cm⁻³.

Collection number ICSD 29

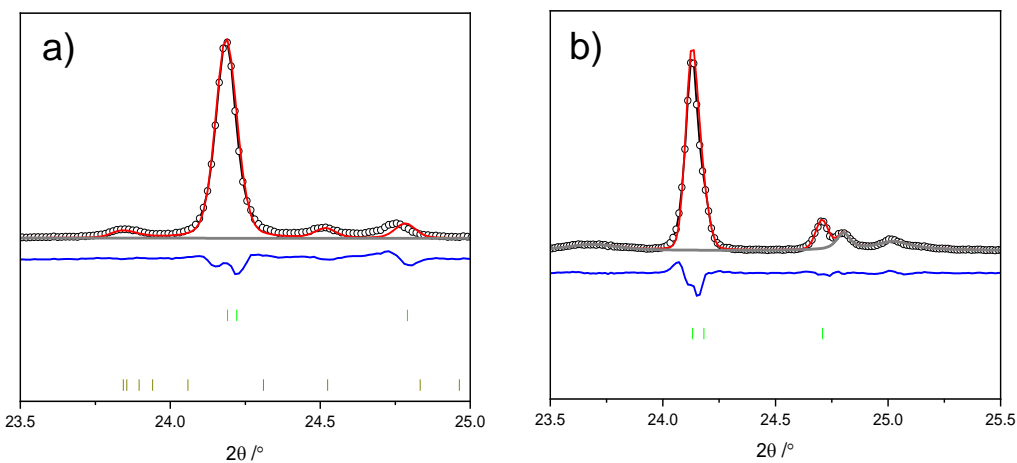


Figure S6: a) MNO-Li zoomed PXRD data showing some of Nb_2O_5 diffraction peaks, and b) MNO-Na showing some of the reflection peaks of the impurities added to as background.

Table S3: Diffraction peaks added as background in the Rietveld refinement against MNO-Na data.

Peak position ($^{\circ}$)	Intensity (a.u.)	σ	γ
18.5434	7643.621	4.032	7.582
18.6904	8478.702	2.374	11.827
23.6916	34875.230	35.325	20.468
24.8007	23123.664	4.859	4.859
25.0242	32712.987	17.805	17.805
25.0100	16597.900	687.092	71.470
32.2414	42652.968	1459.669	84.965
44.1296	17661.259	608.154	38.264
53.8177	5275.315	545297.533	0.082
58.3694	16868.079	5.344	36.337

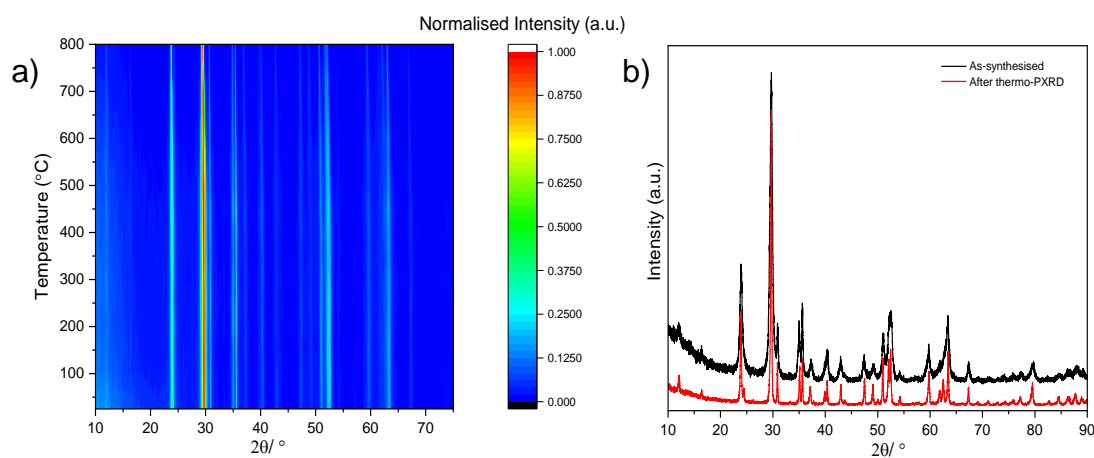


Figure S7: Thermo-PXRD obtained from a) heating CMNO at room temperature up to 800 $^{\circ}\text{C}$ in air, and b) PXRD pattern before and after heating.

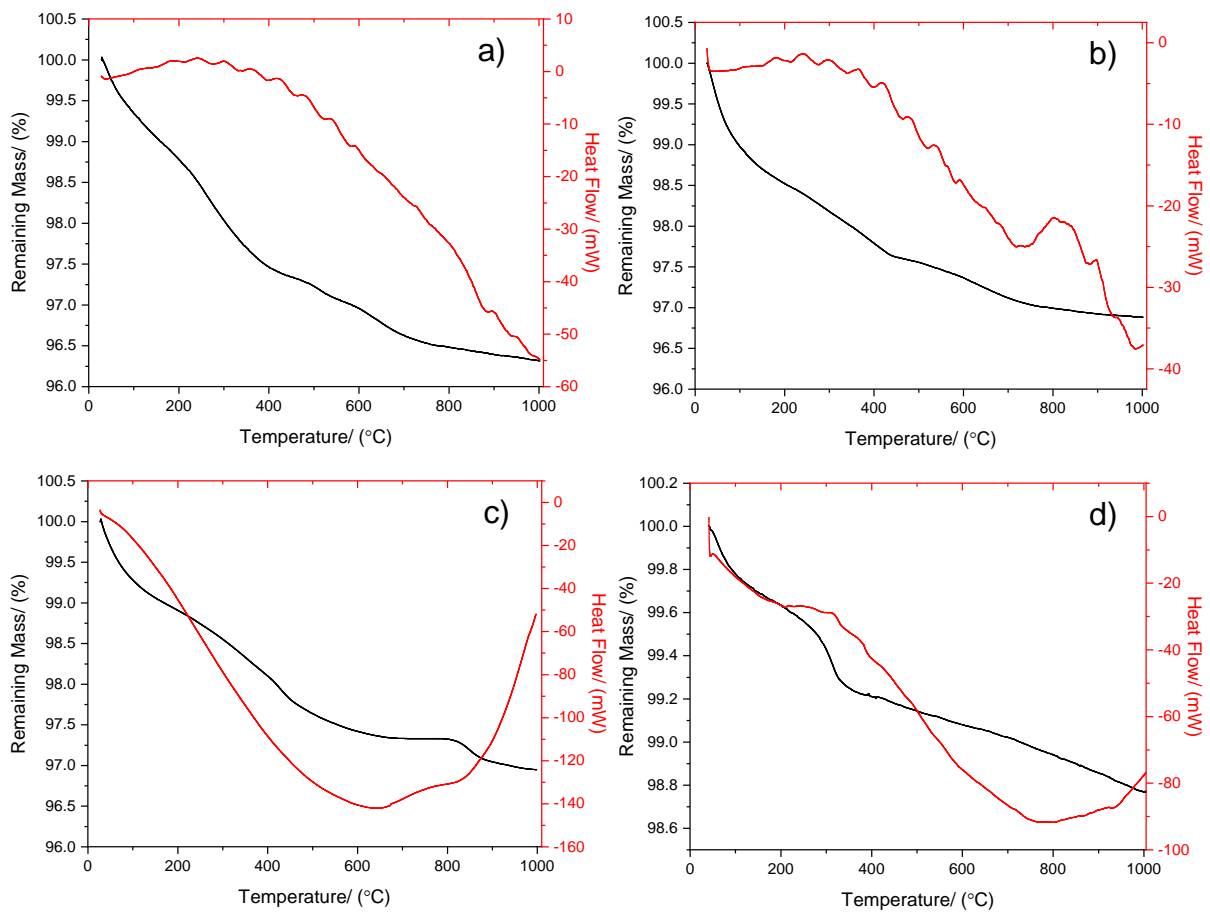


Figure S8: Thermogravimetric analysis of as-synthesised samples a) MNO-Li, b) MNO-Na, c) MNO-K, and d) CMNO.

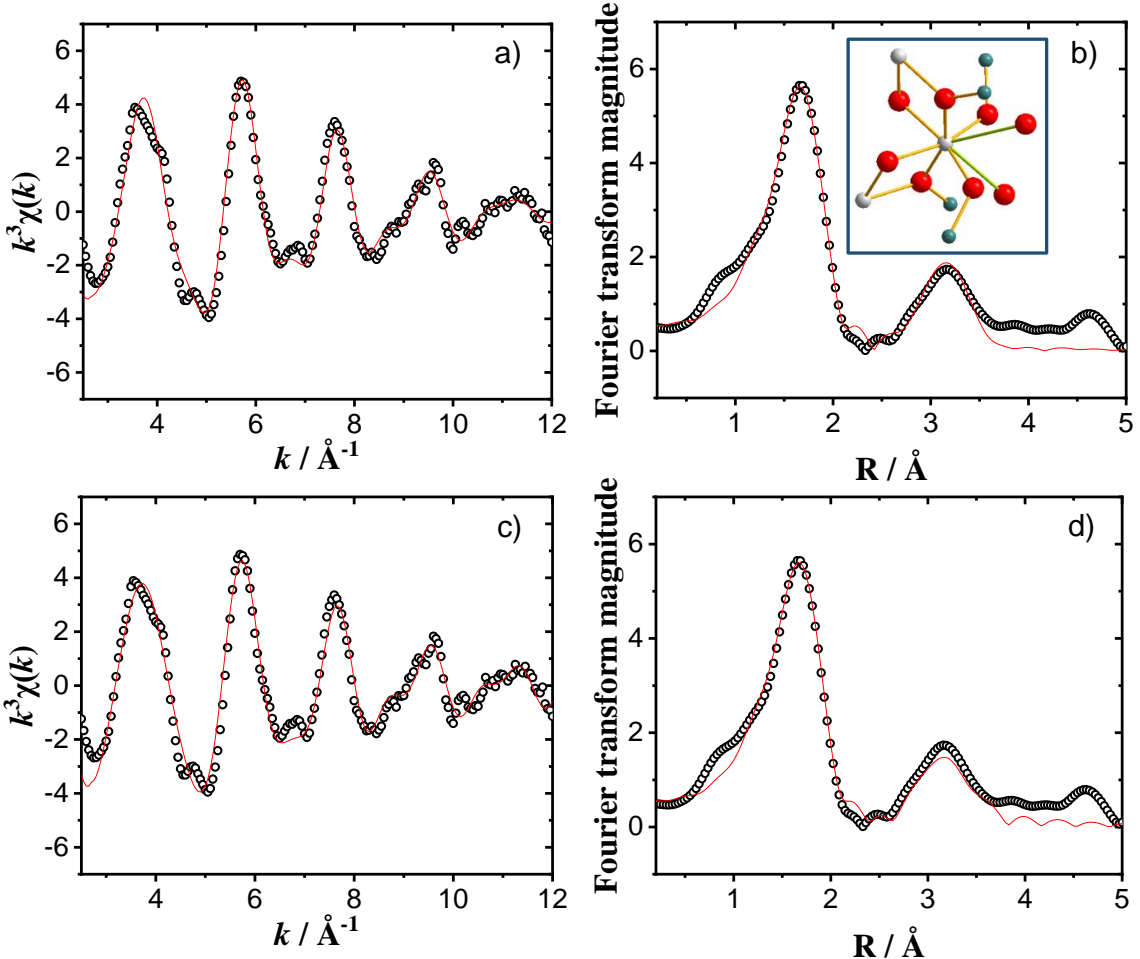


Figure S9: Fits of Mn K-edge EXAFS for ordered model a) $k^3\chi(k)$, b) Fourier transform magnitude, and disordered model, c) $k^3\chi(k)$, and d) Fourier transform magnitude. Open symbols represent data, and the red line the fit. Insert on Fig. S9b represents the first and second shells of an ordered columbite, Mn (in white), Nb (in green), O (in red)⁴, which was modified to a disordered structure.

Table S4: Mn K-edge EXAFS fitted parameters of ordered MnNb_2O_6 (MNO-Li) and disordered $(\text{Mn}_{0.5}\text{Nb}_{0.5})(\text{Mn}_{0.5}\text{Nb}_{1.5})\text{O}_6$ models showing the atomic distance and σ^2 values (R-factor = 0.0444361 and 0.0407176, respectively). The shell occupancy was fixed during refinement of other parameters, and expected distances are shown for MnNb_2O_6 .

Atom	Shell Occupancy	Distance / Å	σ^2 / Å ²
Ordered model			
O ₁	6	2.13(1)	0.0108(7)
O ₂	2	3.08(3)	0.006(5)
Mn	2	3.33(3)	0.014(5)
Nb	4	3.58(3)	0.018(5)
Disordered model			
O	6	2.138(16)	0.0109(10)
O	2	3.058(44)	0.0063(65)
Mn	1	3.452(29)	0.0056(33)
Nb	1	3.625(29)	0.0056(33)
Mn	2	3.302(30)	0.0102(40)
Nb	2	3.475(30)	0.0102(40)
Expected Distances MnNb_2O_6 (ICSD: 15856)			
Atom	Distance / Å		
O ₁	2.0719		
O ₂	2.1919		
O ₃	2.2873		
Mn	3.3569		
Nb ₁	3.5215		
Nb ₂	3.5376		

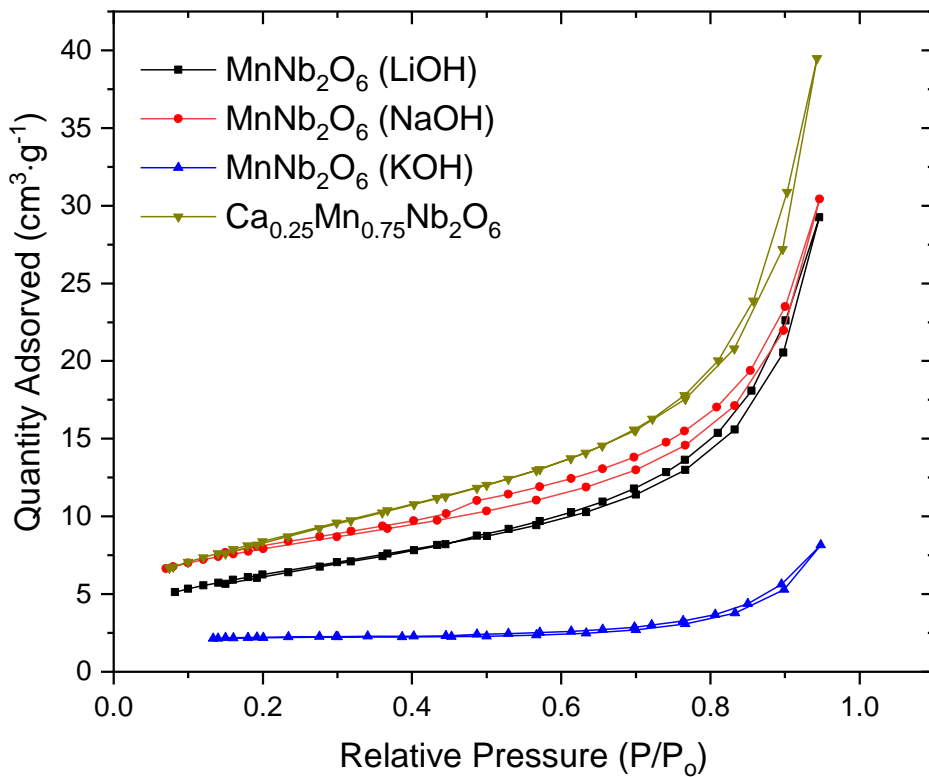


Figure S10: N₂ absorption isotherms for the as-synthesised samples MnNb₂O₆ from Li, Na and K hydroxides and Ca_{0.25}Mn_{0.75}Nb₂O₆.

Table S5: Average pore size and BET surface area of MnNb₂O₆ from Li, Na and K hydroxides and Ca_{0.25}Mn_{0.75}Nb₂O₆.

Sample	Average Pore Width / (nm)*	BET Surface Area / (m ² ·g ⁻¹)
MNO-Li	8.36	22.64 ± 0.07
MNO-Na	8.19	27.97 ± 0.17
MNO-K	13.75	7.06 ± 0.11
CMNO	8.15	30.47 ± 0.04

*Desorption pore diameter

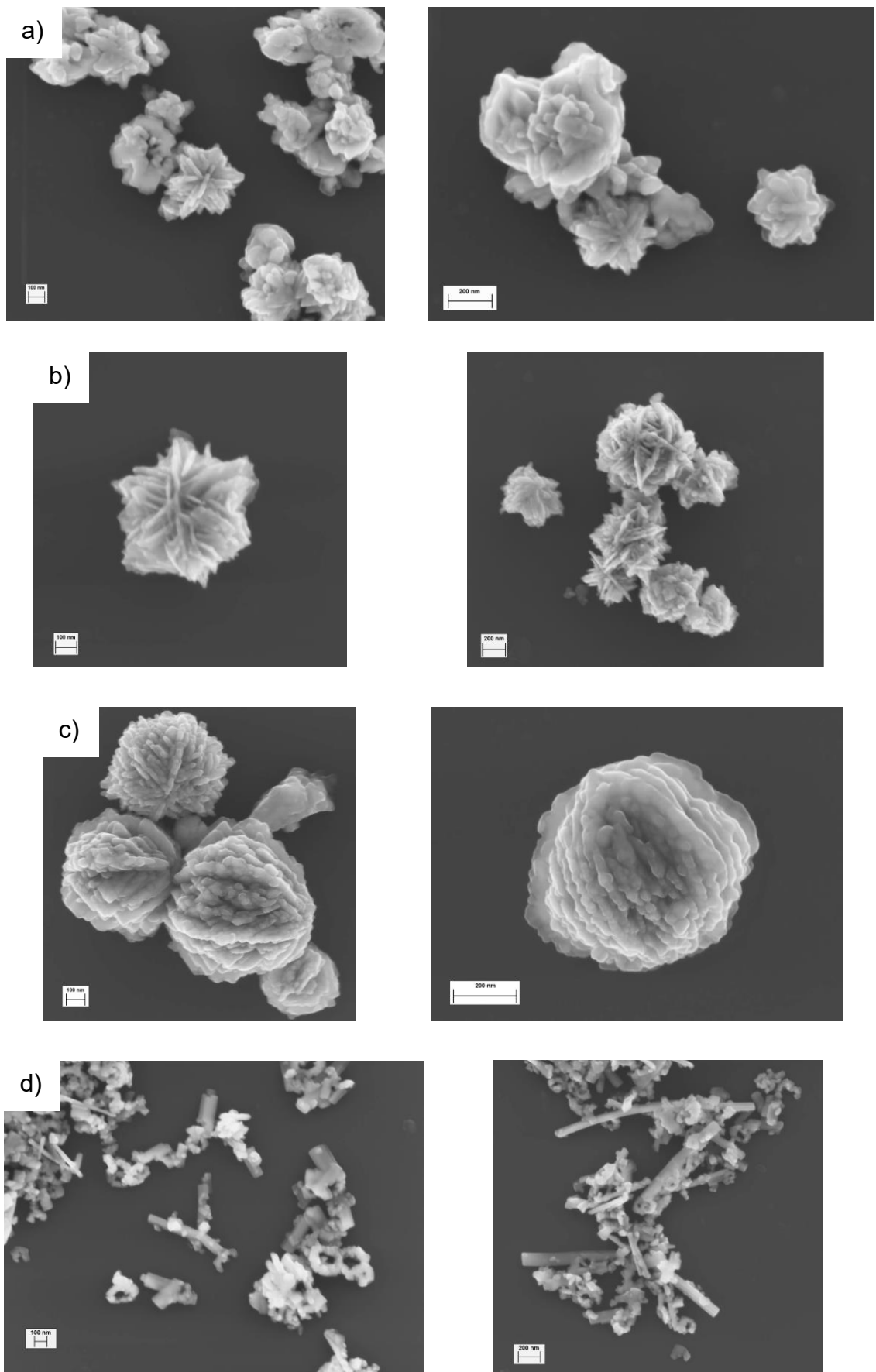


Figure S11: SEM images from hydrothermally synthesised Mn columbite samples using a) LiOH, b) NaOH, c) KOH and d) $\text{Ca}_{0.25}\text{Mn}_{0.75}\text{Nb}_2\text{O}_6$ from small batches. Images (left) are at a scale of 100 nm, and 200 nm (right). Carbon coated (10 nm) particles, 5 kV, InLens detector and working distance between 3–6 mm.

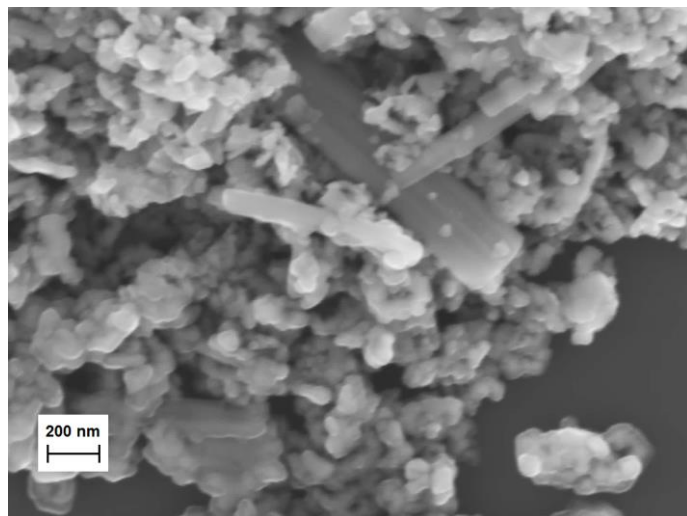


Figure S12: $\text{Ca}_{0.25}\text{Mn}_{0.75}\text{Nb}_2\text{O}_6$ SEM image, highlighting the rods mixed with small undefined shaped particles. Carbon coated (10 nm) particles, 5 kV, and InLens detector and working distance of 5.1 mm. Scale bar equals to 200 nm.

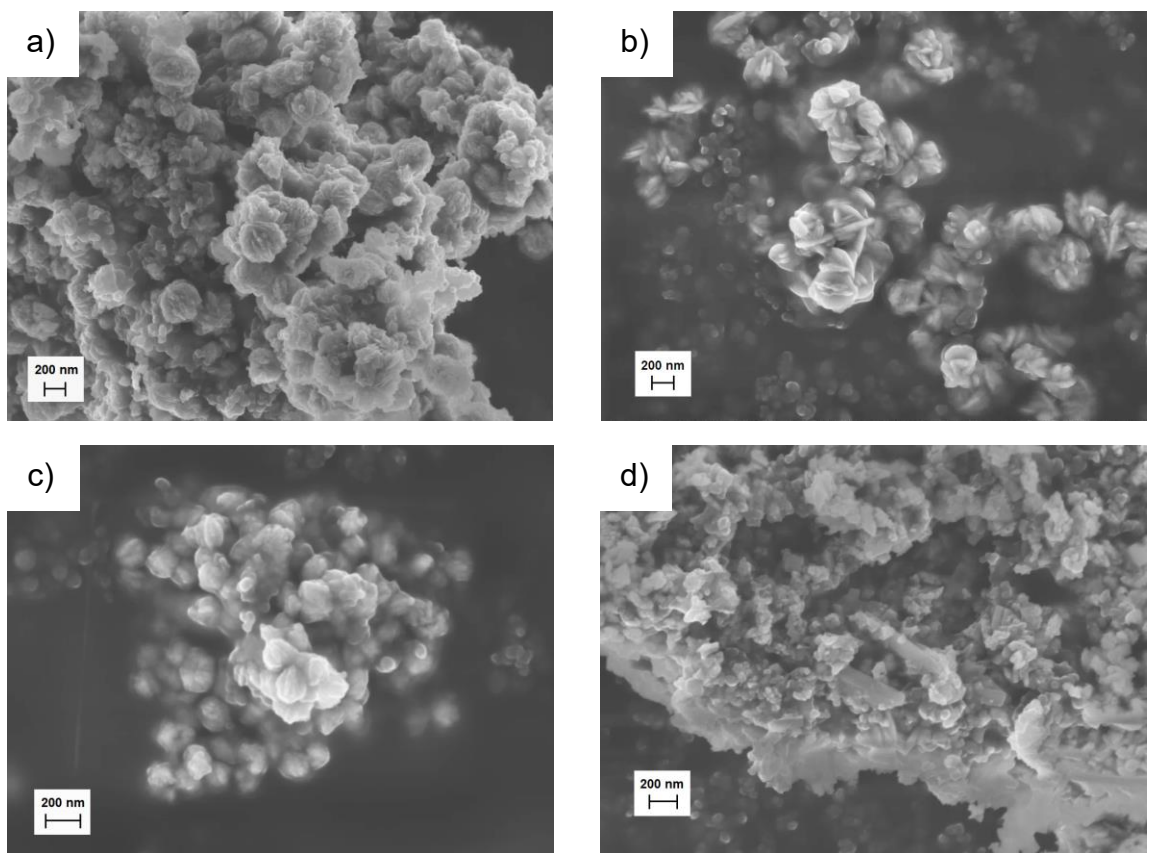


Figure S13: MnNb₂O₆ SEM images of ball milled oxides with 5 wt% carbon black from a) Li, b) Na, c) K hydroxides, and d) Ca_{0.25}Mn_{0.75}Nb₂O₆. Samples were analysed after ball milling without any further coating using an acceleration voltage of 5 kV, InLens detector, and working distance between 3.5–5.0 mm. Scale bars equal to 200 nm.

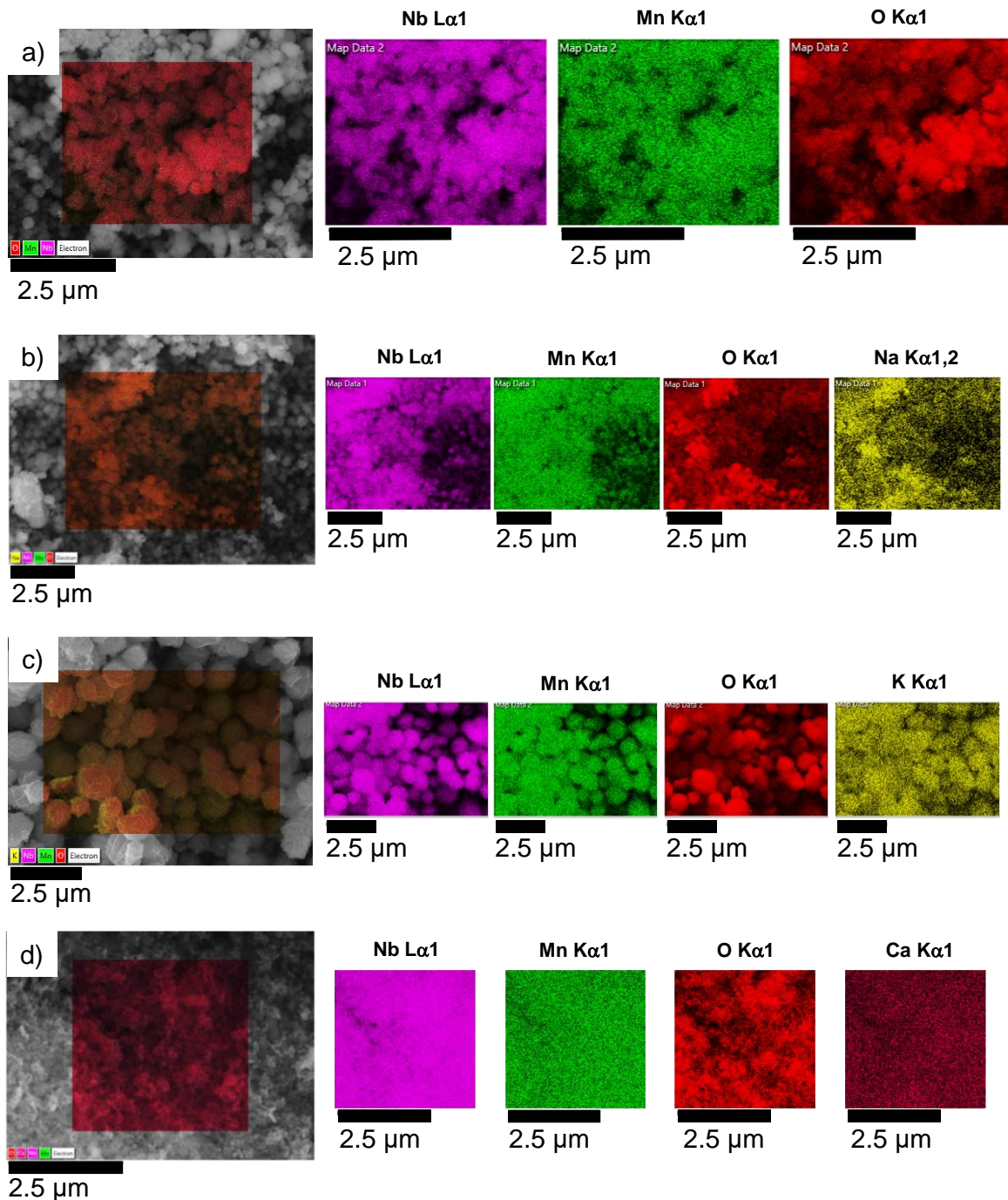


Figure S14: EDS elemental maps for MnNb₂O₆ from a) LiOH, b) NaOH, C) KOH, and d) Ca_{0.25}Mn_{0.75}Nb₂O₆. Carbon tabs, highly covered in powder. Nb L_α1 (pink), Mn K_α1 (green), O K_α1 (red), Na K_α1,2 or K_α1 (yellow) and Ca K_α1 (dark pink).

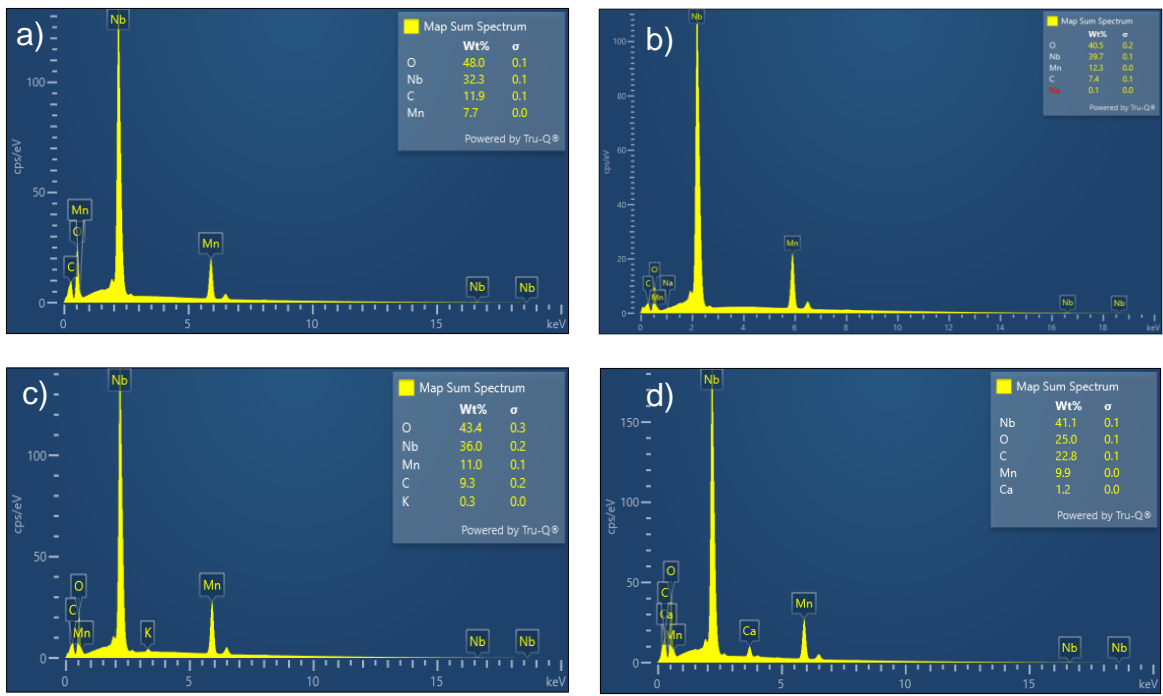


Figure S15: As-made MnNb₂O₆ EDS spectra and mapping for Mn, Nb and other elements from a) Li, b) Na and c) K hydroxides, and d) Ca_{0.25}Mn_{0.75}Nb₂O₆. Carbon tabs highly covered in powder, 15 kV, SE2 detector and working distance between 8–10 mm.

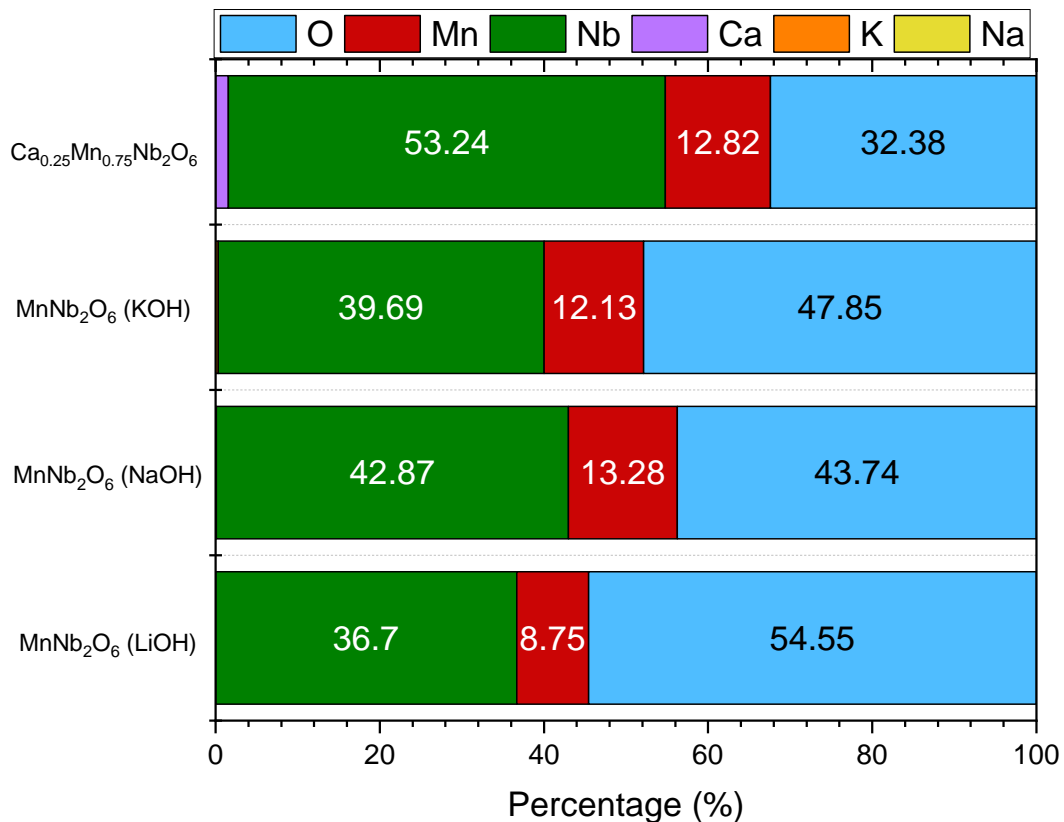


Figure S16: Calculated percentage of elements present in the as-synthesised samples, using the EDS wt% for each element. Na and K percentages equal to 0.1 and 0.3%. The chemical formulae are $\text{Mn}_{0.81}\text{Nb}_2\text{O}_{5.81}$, $\text{Na}_{0.02}\text{Mn}_{1.05}\text{Nb}_2\text{O}_{6.06}$, $\text{K}_{0.04}\text{Mn}_{1.04}\text{Nb}_2\text{O}_{6.06}$, $\text{Ca}_{0.14}\text{Mn}_{0.81}\text{Nb}_2\text{O}_{5.95}$ by using metal ratios to calculate the oxygen stoichiometry.

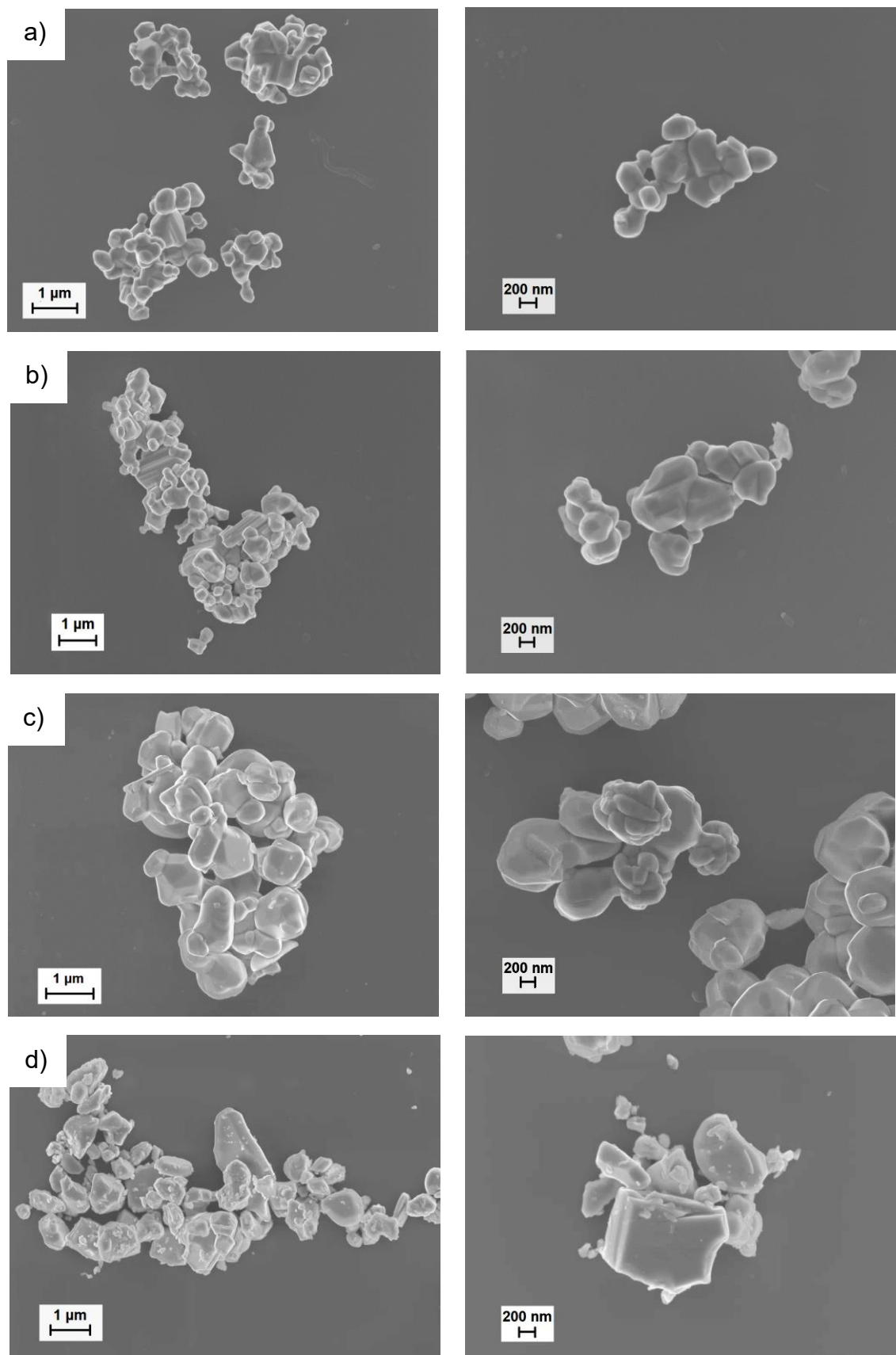


Figure S17: SEM images from sintered Mn columbite samples using a) LiOH, B) NaOH, c) KOH and d) CMNO. Images are at a scale of 1 μm (left), and 200 nm (right). Carbon coated (10 nm) particles, 4 kV, InLens detector and working distance of 5.3 mm. Samples were sonicated in IPA for 5 min and drop casted onto Si wafers.

Table S6: XRF analyses displaying the mass percentage of Na, K, Ca, Mn and Nb oxides present in the as-synthesised samples.

Sample	Na (%)	K (%)	Ca (%)	Mn (%)	Nb (%)
MNO-Li	-	-	-	25.28	74.55
MNO-Na*	0.11	-	-	7.00	30.25
MNO-K	-	0.61	-	20.92	78.38
CMNO	-	-	2.21	16.49	81.23

*MnNb₂O₆ from NaOH measured as a pellet. Polyethylene film absorbs lower-energy X-rays and elements lighter than Cl can not be detected.

Table S7: Elemental analysis for all metals (wt%) presents in the synthesised materials from EDS and XRF measurements and comparison with the composition refined from the PXRD data before and after heat treatment.

Measurement	Sample	Na (%)	K (%)	Ca (%)	Mn (%)	Nb (%)
XRF	MNO-Li	-	-	-	36.5	63.5
	MNO-Na	1.1	-	-	27.7	71.2
	MNO-K	-	1.4	-	30.6	68.0
	CMNO	-	-	4.6	24.5	70.9
EDS	MNO-Li	-	-	-	28.8	71.2
	MNO-Na	0.7	-	-	34.2	65.1
	MNO-K	-	1.3	-	33.8	64.9
	CMNO	-	-	4.7	27.5	67.8
Refined	MNO-Li*	-	-	-	36.7	63.3
	MNO-Na*	-	-	-	40.8	59.2
	MNO-K*	-	-	-	37.2	62.5
	CMNO	-	-	4.3	29.0	66.7
Refined	Measurement	Sintered samples				
	MNO-Li	-	-	-	37.6	62.4
	MNO-Na	-	-	-	33.3	66.7
	MNO-K	-	-	-	33.3	66.7
	CMNO	-	-	7.3	26	66.7

*Refinements used an ixiolite model.

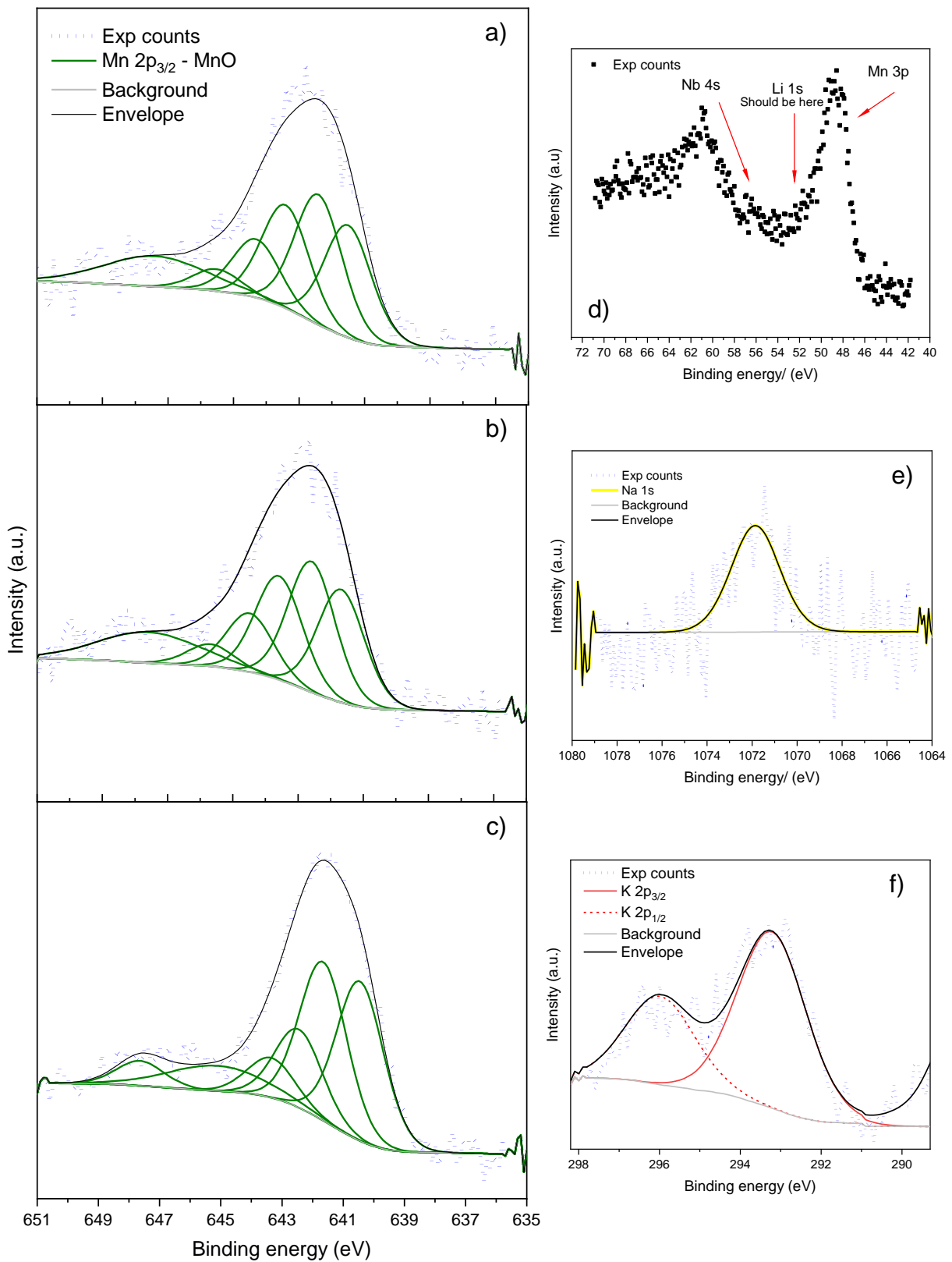


Figure S18: XPS spectra of Mn 2p_{3/2} region of MnNb₂O₆ made from a) Li and b) Na hydroxides, c) sintered sample from K hydroxide, and data from the alkaline metals d) Li 1s, e) Na 1s and f) K 2p_{3/2} and 2p_{1/2}.

Table S8: XPS results: O 1s (metal oxides) and Nb 3d spin orbit split states ($3d_{5/2}$ and $3d_{3/2}$) binding energies of as-made MnNb_2O_6 (LiOH, NaOH), sintered MnNb_2O_6 (KOH). Literature values of Nb oxide standards, Li_3NbO_4 , NaNbO_3 , Nb_2O_5 and NbO_2 , are included for comparison.

Sample	Energy of O 1s (metal oxides) and Nb 3d sites						
	O 1s (TM-O)	Nb(1) $3d_{5/2}$	Nb(1) $3d_{3/2}$	Nb(2) $3d_{5/2}$	Nb(2) $3d_{3/2}$	Nb(3) $3d_{5/2}$	Nb(3) $3d_{3/2}$
Binding Energy / (eV)							
MnNb_2O_6 (LiOH)	529.99	208.14	210.86	206.90	209.62	-	-
MnNb_2O_6 (NaOH)	530.14	208.36	211.08	207.17	209.89	-	-
MnNb_2O_6 (KOH) sintered	530.04	207.82	210.54	206.76	209.53	-	-
Li_3NbO_4	530.44	208.43	211.15	207.46	210.23	-	-
NaNbO_3	530.64	208.62	211.34	207.37	210.14	-	-
NaNbO_3^5	529.9	207.1	-	-	-	-	-
Nb_2O_5	530.63	207.79	210.51	206.48	209.25	-	-
Nb_2O_5^5	530.8						
NbO_2	530.30	-	-	207.19	209.96	205.44	208.16
NbO_2^5	531.03	-	-	-	-	206	-
$\text{MnNb}_2\text{O}_6^6$	530.0			207.0	209.8		
$\text{MnNb}_2\text{O}_6^7$	■			206.6	209.2		
$\text{MnNb}_2\text{O}_6^8$	530.1			206.8	209.4		
$\text{MnNb}_2\text{O}_6^9$	*			206.8	209.4		
$\text{MnNb}_2\text{O}_6^{10}$	530.1			▼	▼	▼	▼

■ Only O 1s spectrum was showed. No fitting reported. * O1s data was not reported. ▼ No fitting for Nb $3d_{5/2}$ and $3d_{3/2}$.

Table S9: Calculated energy separation between O 1s (metal oxides) and Nb 3d spin orbit split states ($3d_{5/2}$ and $3d_{3/2}$).

Sample	Energy separation between O 1s (metal oxides) and Nb 3d					
	Nb(1) $3d_{5/2}$	Nb(1) $3d_{3/2}$	Nb(2) $3d_{5/2}$	Nb(2) $3d_{3/2}$	Nb(3) $3d_{5/2}$	Nb(3) $3d_{3/2}$
	Binding Energy / (eV)					
MnNb ₂ O ₆ (LiOH)	321.85	319.13	323.09	320.37	-	-
MnNb ₂ O ₆ (NaOH)	321.78	319.06	322.97	320.25	-	-
MnNb ₂ O ₆ (KOH) sintered	322.22	319.50	323.28	320.51	-	-
Li ₃ NbO ₄	322.01	319.29	322.98	320.21	-	-
NaNbO ₃	322.02	319.30	323.27	320.50	-	-
NaNbO ₃ ⁵	322.8	-	-	-	-	-
Nb ₂ O ₅	322.84	320.12	324.15	321.38	-	-
Nb ₂ O ₅ ⁵	323.1	-	-	-	-	-
NbO ₂	-	-	323.11	320.34	324.86	322.14
NbO ₂ ⁵	-	-	-	-	325.03	-
MnNb ₂ O ₆ ⁶	-	-	323	320.2	-	-
MnNb ₂ O ₆ ⁸	-		323.3	320.7		

XPS spectra and PXRD patterns - Reference materials

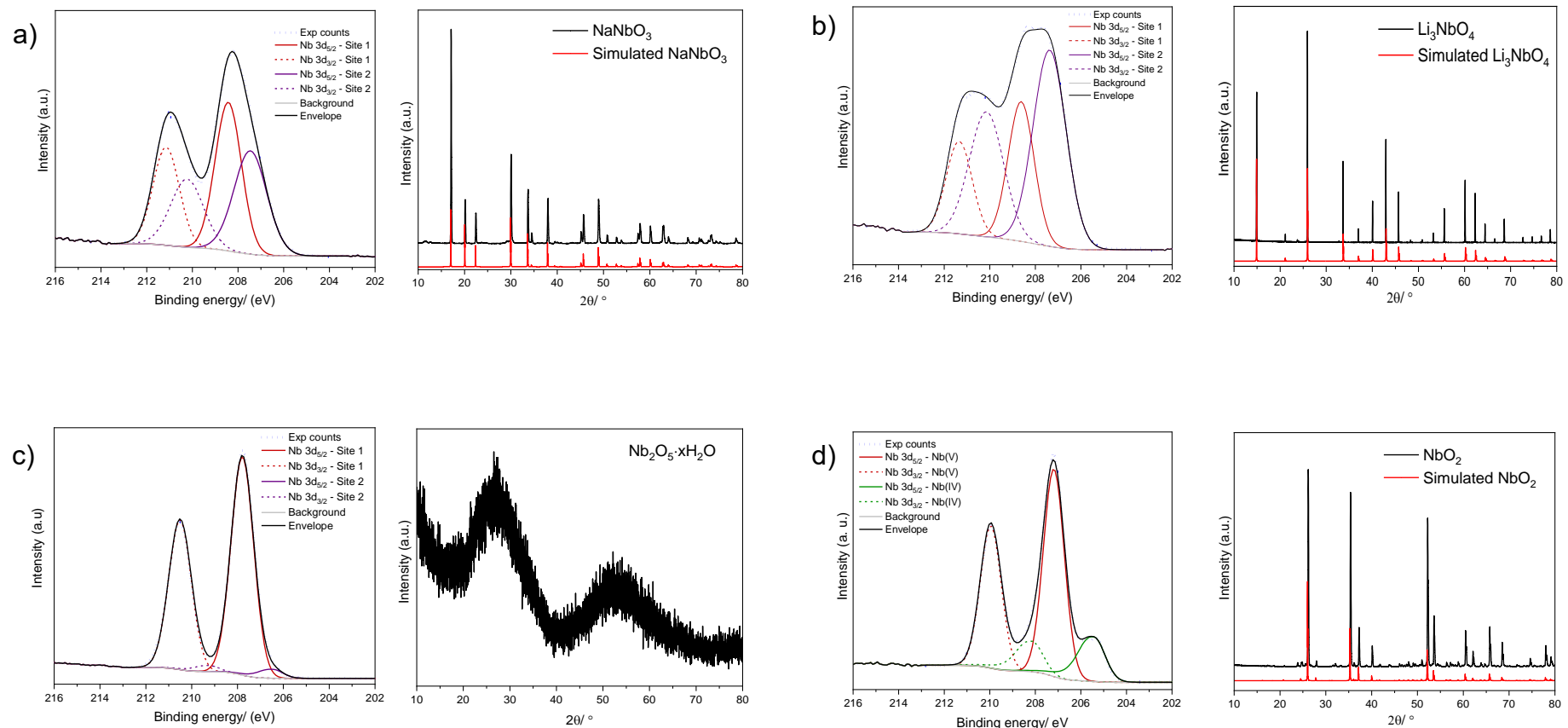


Figure S19: XPS spectra from different Nb standards and their corresponding PXRD: a) NaNbO_3 , b) Li_3NbO_4 , c) Nb_2O_5 (from CBMM) and d) NbO_2 (from Sigma Aldrich).

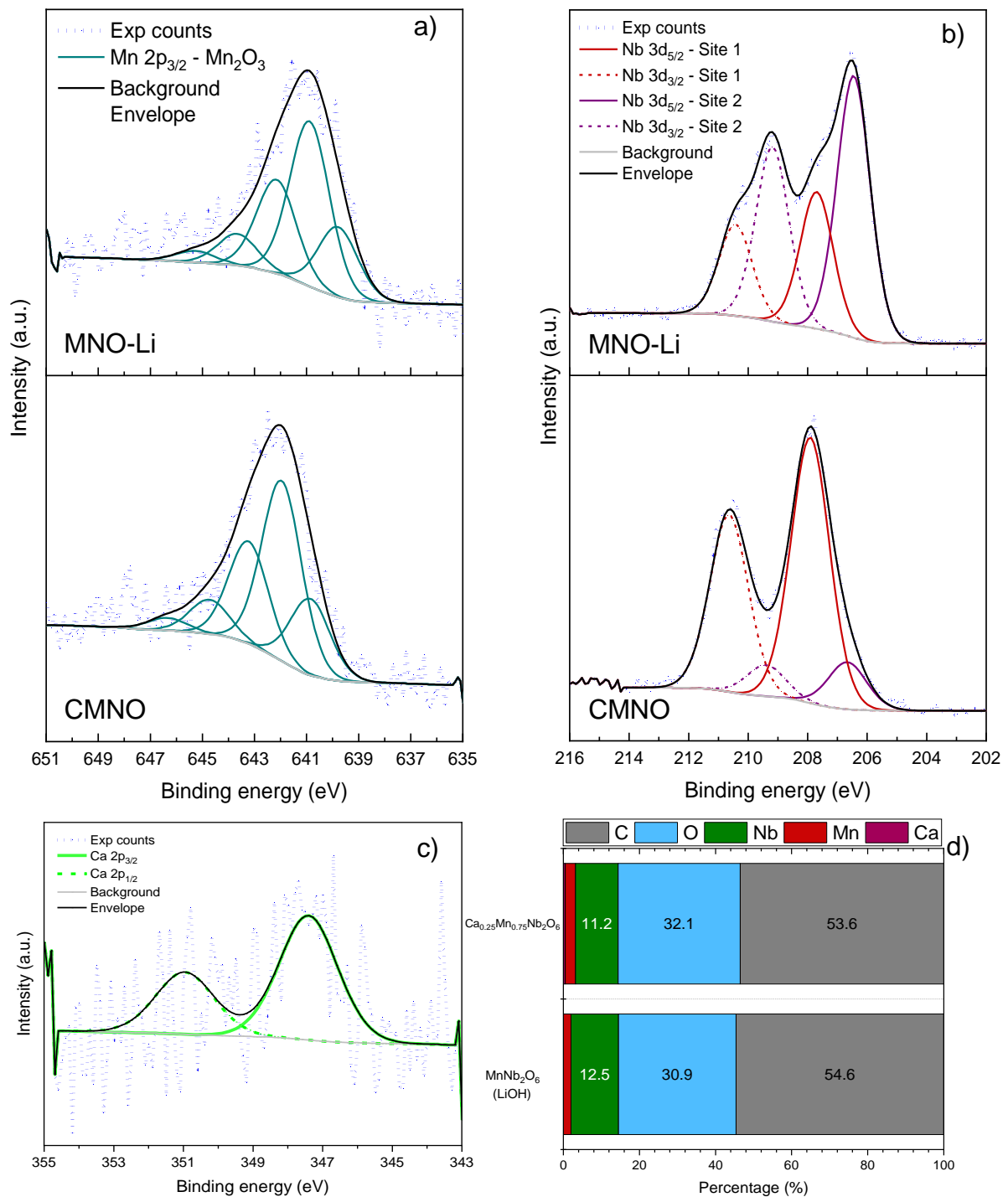


Figure S20: XPS spectra from ball milled MNO-Li and CMNO with C65 (carbon black) showing a) Mn 2p_{3/2}, b) Nb 3d_{5/2} and 3d_{3/2}, c) Ca 2p_{3/2} and 2p_{1/2} (CMNO), and d) surface elemental composition in element percentage.

Table S10: XPS results: O 1s (metal oxides) and Nb 3d spin orbit split states ($3d_{5/2}$ and $3d_{3/2}$) binding energies of as-made MnNb_2O_6 (LiOH and NaOH) and sintered MnNb_2O_6 (KOH) compared to ball-milled samples MnNb_2O_6 (LiOH) and $\text{Ca}_{0.25}\text{Mn}_{0.75}\text{Nb}_2\text{O}_6$ with C65.

Sample	Energy of O 1s (metal oxides) and Nb 3d sites				
	O 1s (TM-O)	Nb(1) $3d_{5/2}$	Nb(1) $3d_{3/2}$	Nb(2) $3d_{5/2}$	Nb(2) $3d_{3/2}$
	Binding Energy / (eV)				
MnNb_2O_6 (LiOH)	529.99	208.14	210.86	206.90	209.62
MnNb_2O_6 (NaOH)	530.14	208.36	211.08	207.17	209.89
MnNb_2O_6 (KOH) sintered	530.04	207.82	210.54	206.76	209.53
Ball milled MnNb_2O_6 (LiOH)	529.55	207.43	210.43	206.45	209.18
Ball milled $\text{Ca}_{0.25}\text{Mn}_{0.75}\text{Nb}_2\text{O}_6$	529.91	207.91	210.64	206.67	209.40

Table S11: Calculated energy separation between O 1s (metal oxides) and Nb 3d spin orbit split states ($3d_{5/2}$ and $3d_{3/2}$).

Sample	Energy separation between O 1s (metal oxides) and Nb 3d			
	Nb(1) $3d_{5/2}$	Nb(1) $3d_{3/2}$	Nb(2) $3d_{5/2}$	Nb(2) $3d_{3/2}$
	Binding Energy / (eV)			
MnNb_2O_6 (LiOH)	321.85	319.13	323.09	320.37
MnNb_2O_6 (NaOH)	321.78	319.06	322.97	320.25
MnNb_2O_6 (KOH) sintered	322.22	319.50	323.28	320.51
Ball milled MnNb_2O_6 (LiOH)	322.12	319.12	323.10	320.37
Ball milled $\text{Ca}_{0.25}\text{Mn}_{0.75}\text{Nb}_2\text{O}_6$	322.00	319.27	323.24	320.51

Table S12: Mass loading of 15 mm electrodes used in the electrochemical tests.

Electrochemical measurement	Average Mass loading ($\text{mg}\cdot\text{cm}^{-2}$)
Cycling 0.005 – 3.0 V	
MNO-Li	4.447 ± 0.667
MNO-Na	3.672 ± 0.299
MNO-K	3.537 ± 0.374
CMNO	3.632 ± 0.175
Current rates 0.005 – 3.0 V	
MNO-Li	4.108 ± 0.162
MNO-Na	3.763 ± 0.062
MNO-K	3.448 ± 0.400
CMNO	3.728 ± 0.211
Cycling 0.5 -2.5 V	
MNO-Li	4.410 ± 0.422
MNO-Na	3.787 ± 0.334
MNO-K	2.879 ± 0.620
CMNO	3.773 ± 0.118
Current rates 0.5 – 2.5 V	
MNO-Li	3.921 ± 0.229
MNO-Na	3.790 ± 0.186
MNO-K	3.171 ± 0.058
CMNO	3.808 ± 0.074

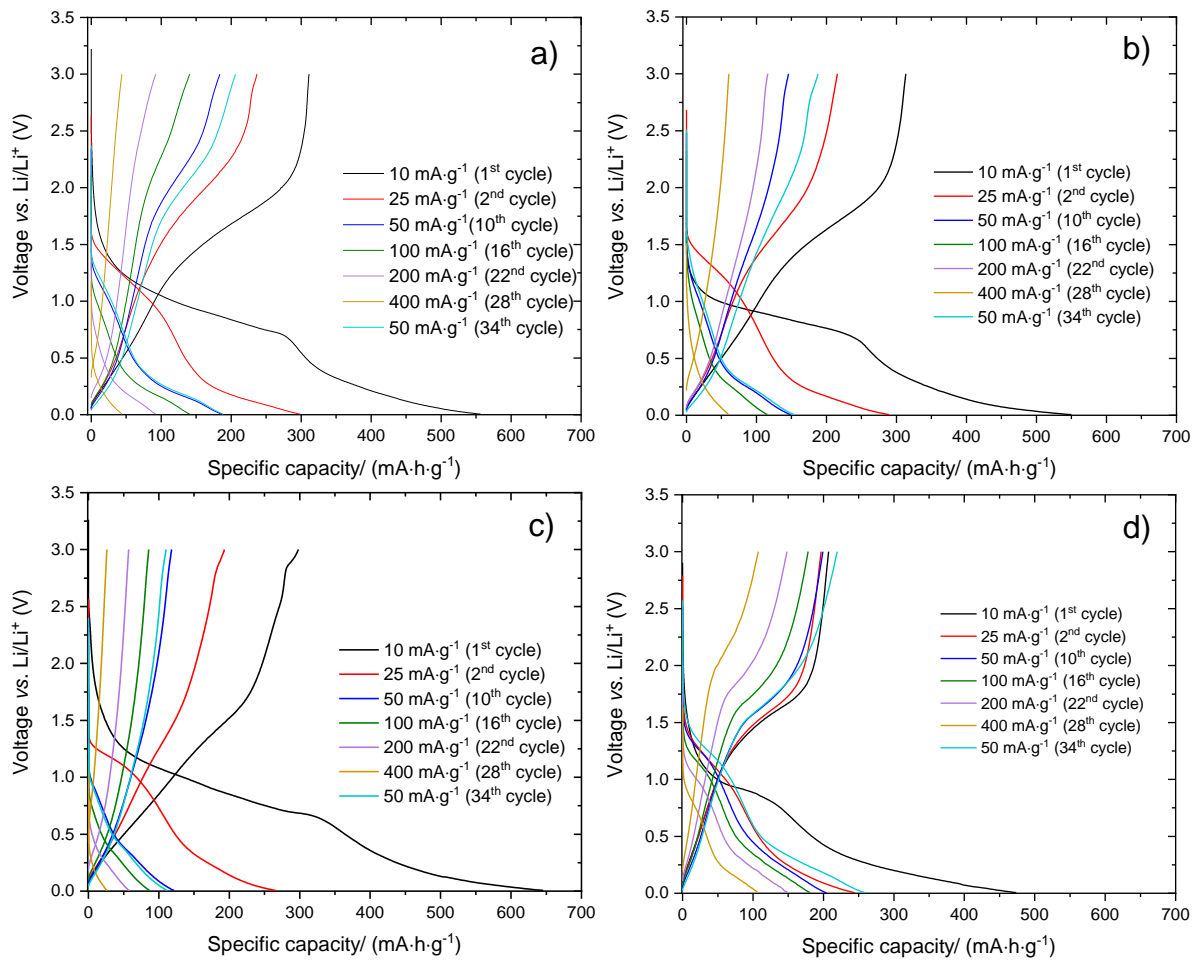


Figure S21: Discharge – charge curves at room temperature under 10 (1st cycle only), 25, 50, 100, 200, 400, and 50 $\text{mA}\cdot\text{g}^{-1}$ for a) MNO-Li, b) MNO-Na, c) MNO-K, and d) CMNO. Voltage window 0.005 – 3.0 V vs. Li/Li^+ .

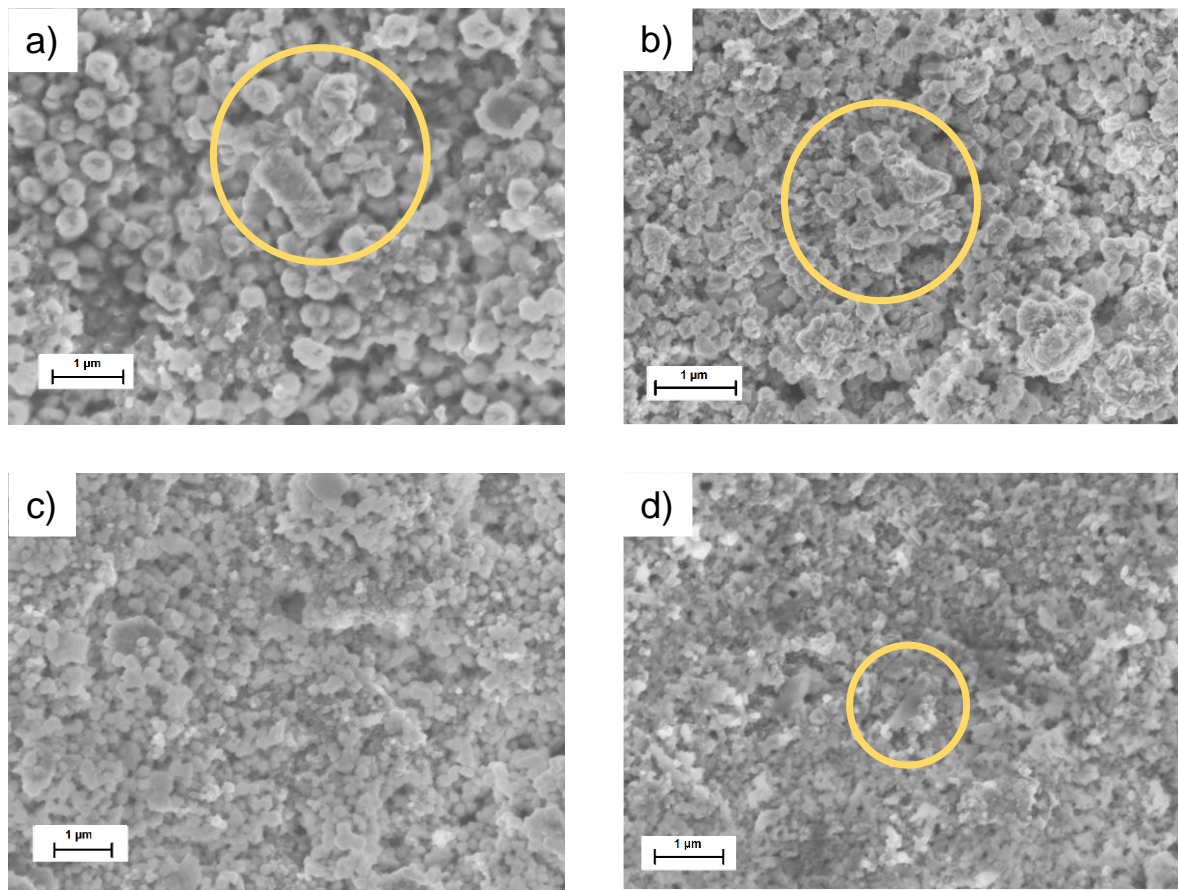


Figure S22: *Ex-situ* SEM images of electrodes after 1st cycle a) MNO-Li, b) MNO-Na, c) MNO-K, and d) CMNO. Yellow circles highlight particles with preserved morphology. 5 kV, InLens detector and working distance between 10–12 mm. Scale bar of 1 μm .

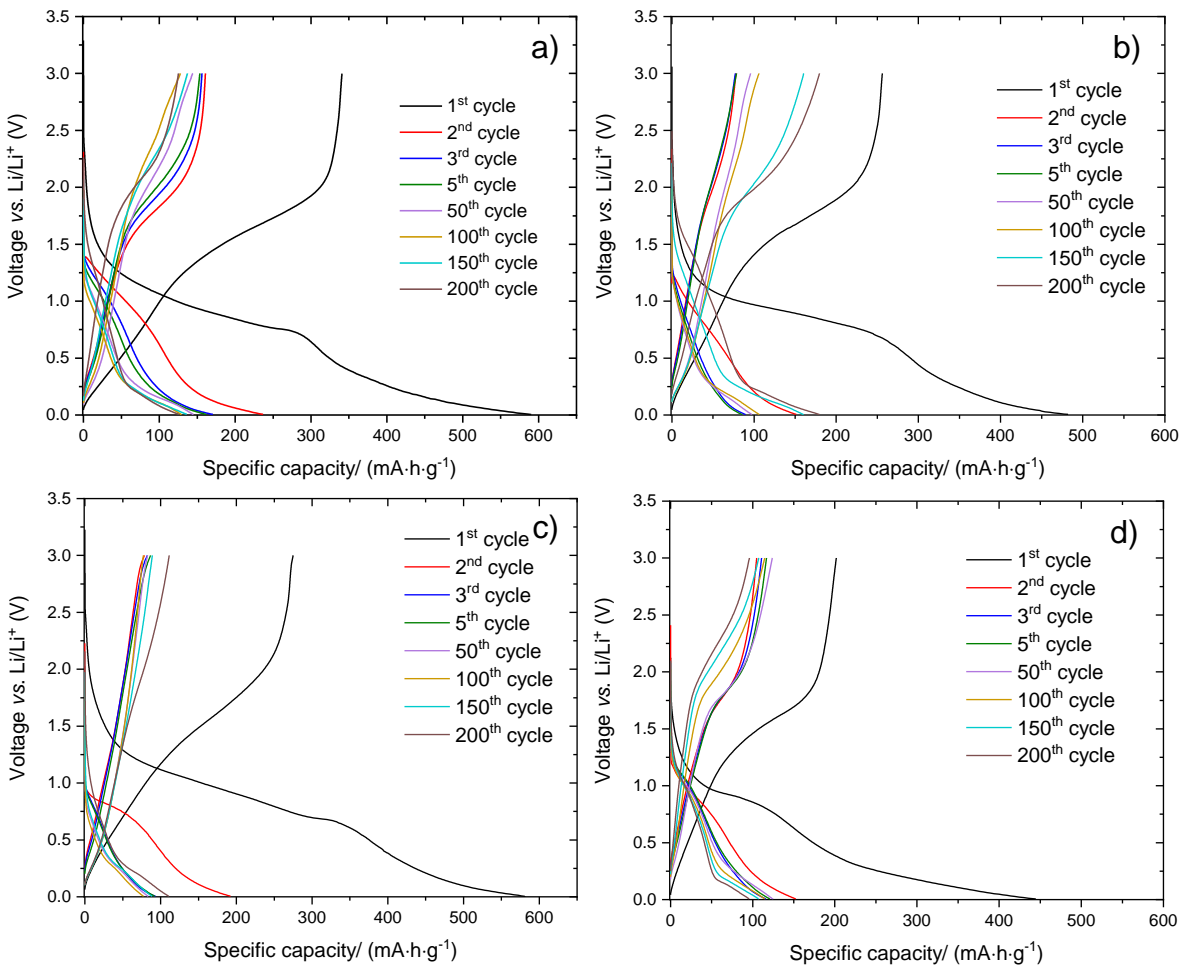


Figure S23: Discharge – charge curves at room temperature 10 (1st cycle only) and 200 (199 cycles) $\text{mA}\cdot\text{g}^{-1}$ for MnNb_2O_6 a) LiOH, b) NaOH, c) KOH and d) $\text{Ca}_{0.25}\text{Mn}_{0.75}\text{Nb}_2\text{O}_6$. Voltage window 0.005 – 3.0 V vs. Li/Li⁺.

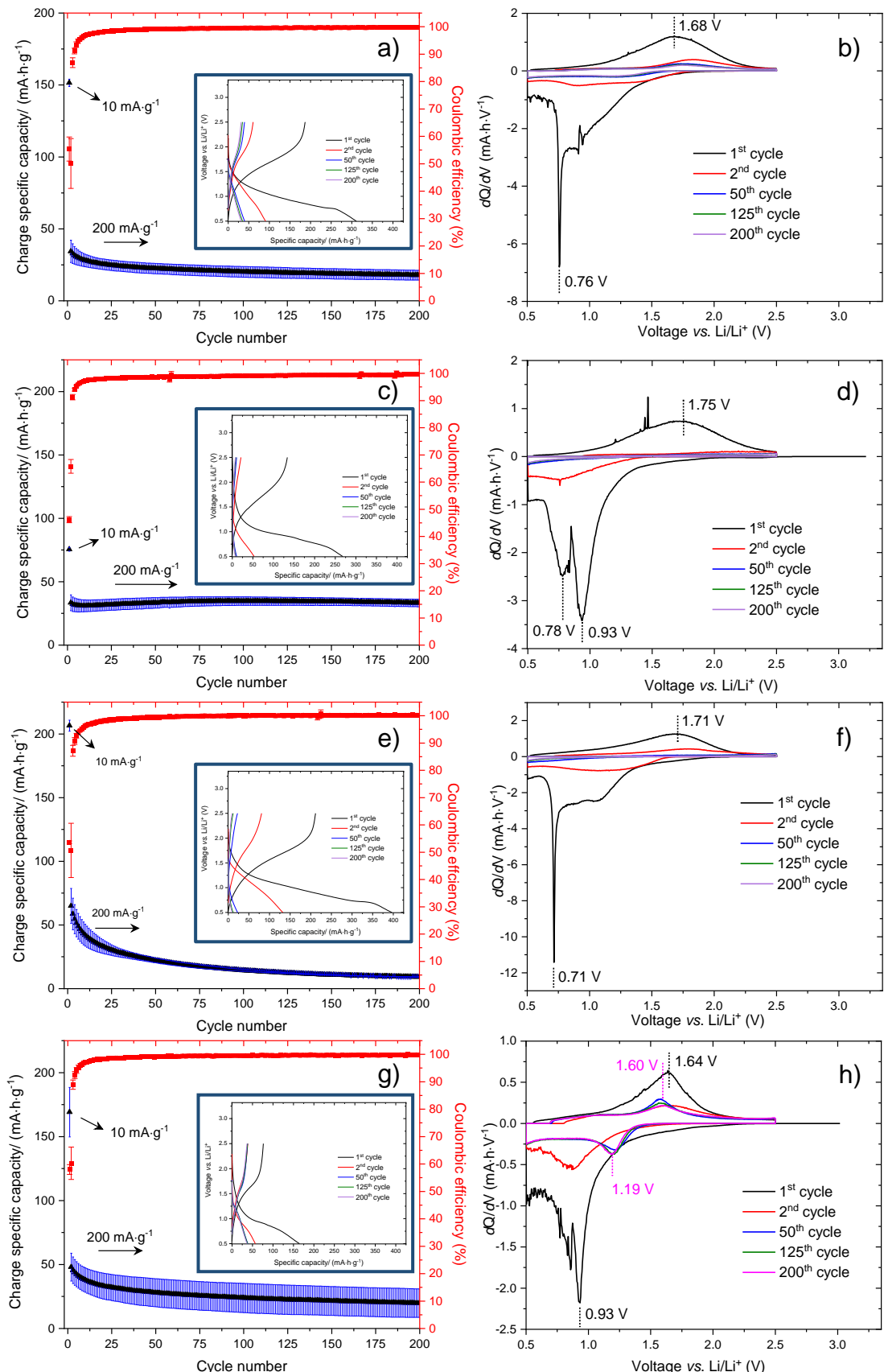


Figure S24: Discharge – charge curves of as-synthesised samples after 200 cycles (1st cycle at 10 mA·g⁻¹ and 199 cycles at 200 mA·g⁻¹) and insert shows the galvanostatic curves under various cycles. (a, c, e, and g) cycling

performance of MNO-Li, MNO-Na, MNO-K, and CMNO. (b, d, f, and h) Differential capacity curves (dQ/dV) of MNO-Li, MNO-Na, MNO-K, CMNO under various cycles. Voltage window between 0.5 – 2.5 V vs. Li/Li⁺.

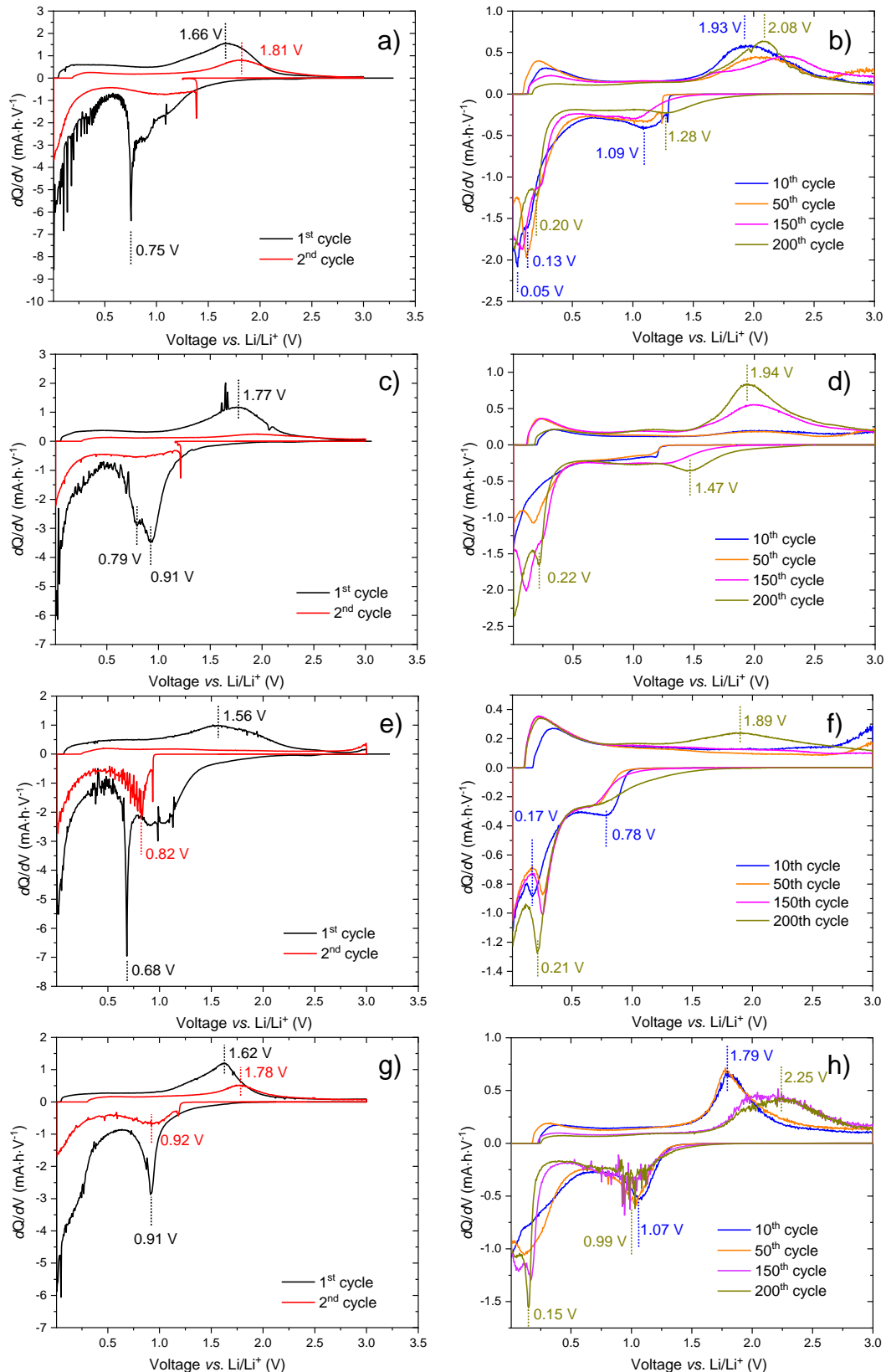


Figure S25: Differential capacity curves (dQ/dV) of MNO-Li, MNO-Na, MNO-K, and CMNO under various cycles. (a, c, e, and g) 1st and 2nd dQ/dV cycles and (b, d, f, and h) 10th, 50th, 150th and 200th dQ/dV cycles. Voltage window between 0.005 – 3.0 V vs. Li/Li⁺.

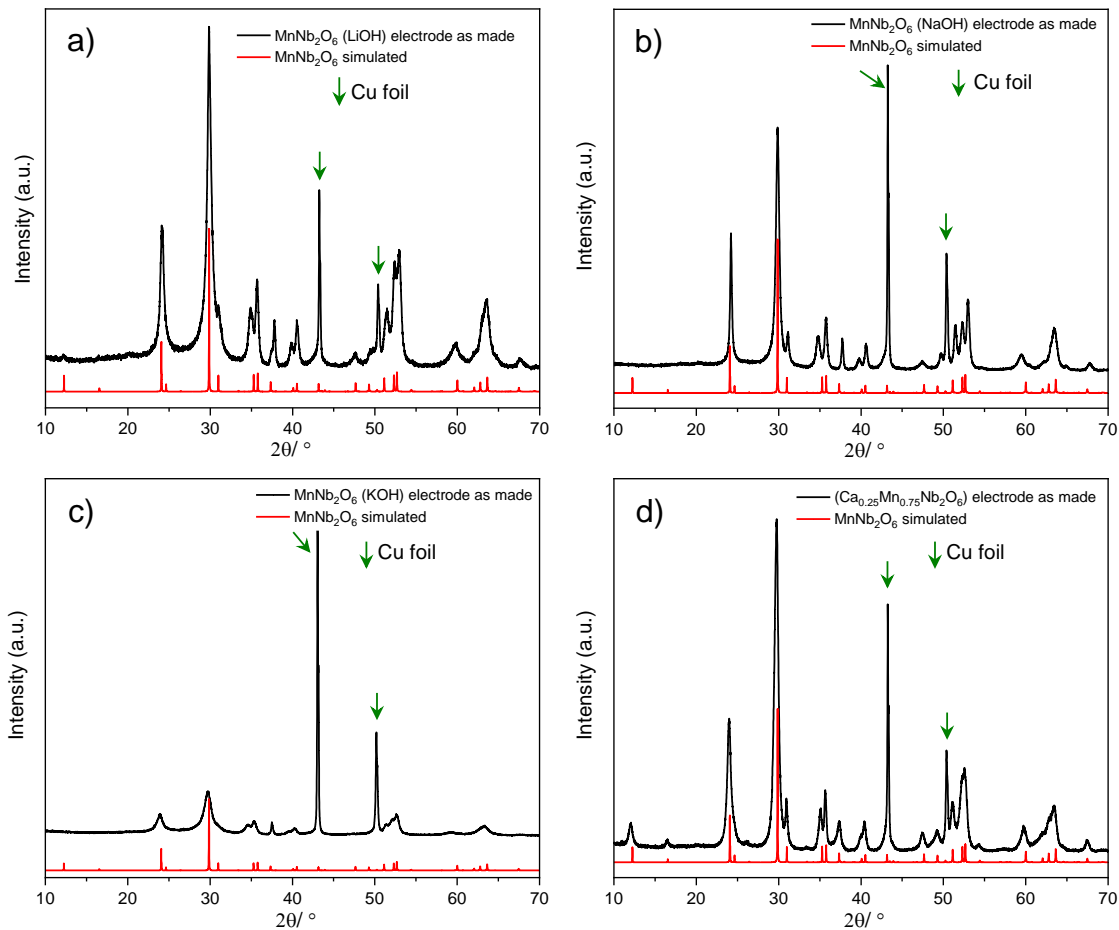


Figure S26: *Ex-situ* diffraction patterns from as-made electrodes a) MNO-Li, b) MNO-Na, c) MNO-K, and d) CMNO.

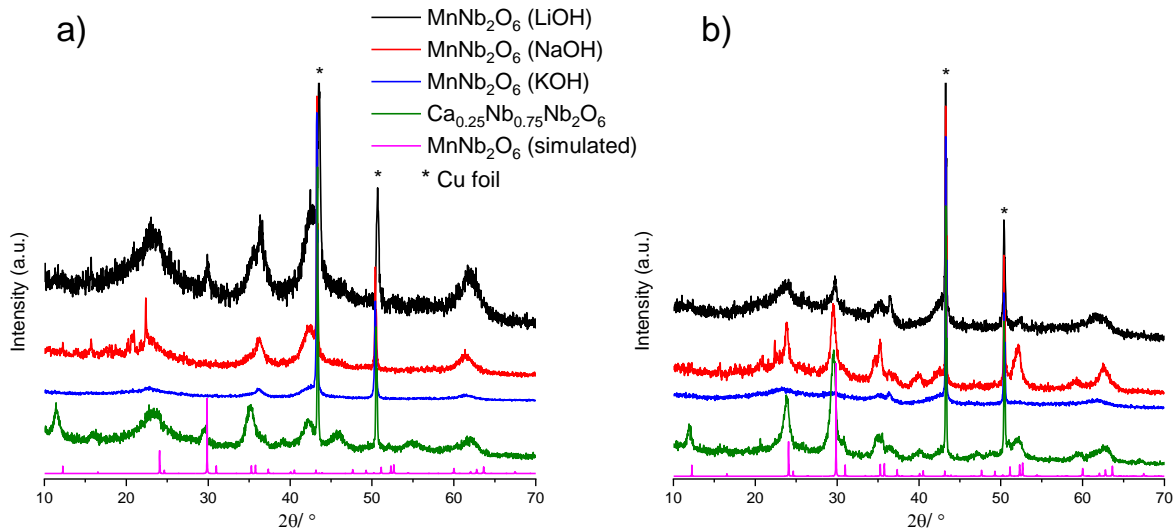


Figure S27: *Ex-situ* PXRD of electrodes discharged to a) 0.005 V and charged to b) 3.0 V.

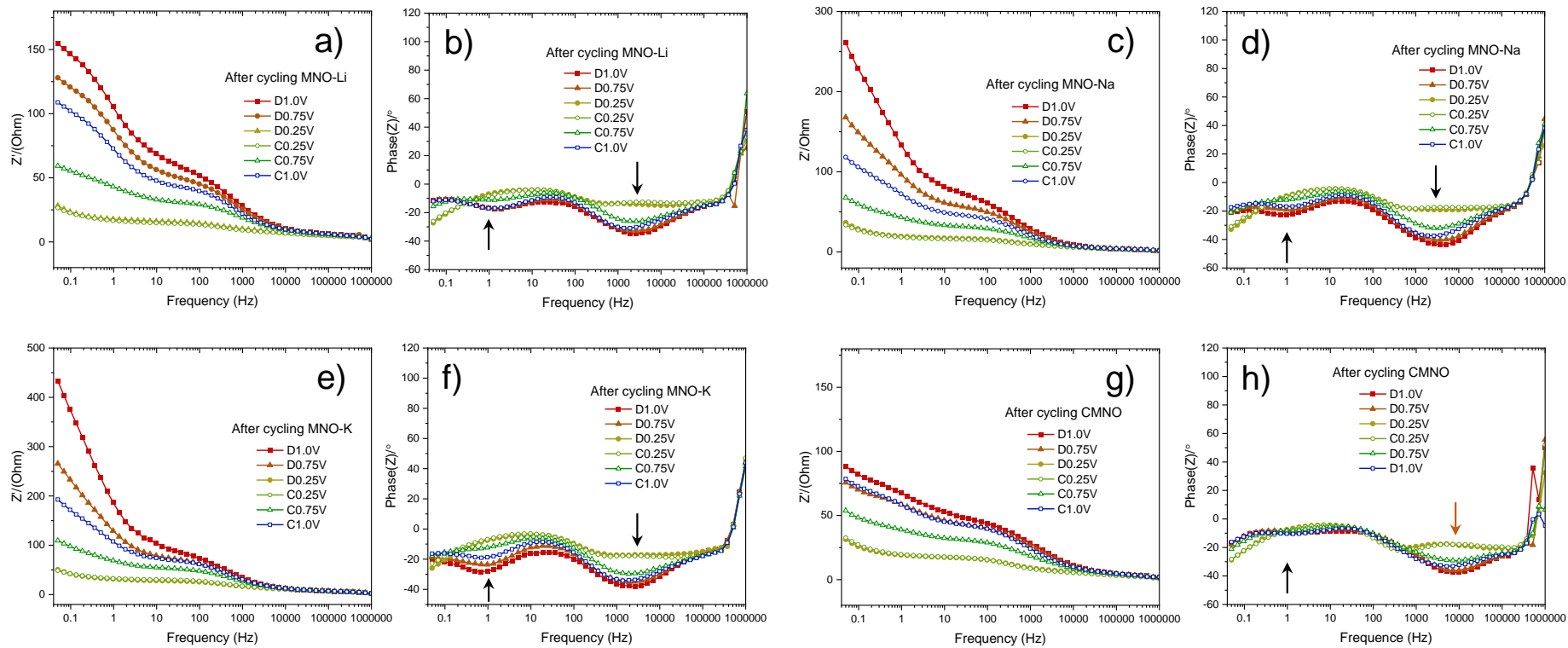


Figure S28: Bode impedance and angle plots of electrodes after 22 cycles (a-b) MNO-Li, (c-d) MNO-Na, (e-f) MNO-K, and (g-f) CMNO. Arrows indicate phase change regions in the active materials during lithiation/delithiation.

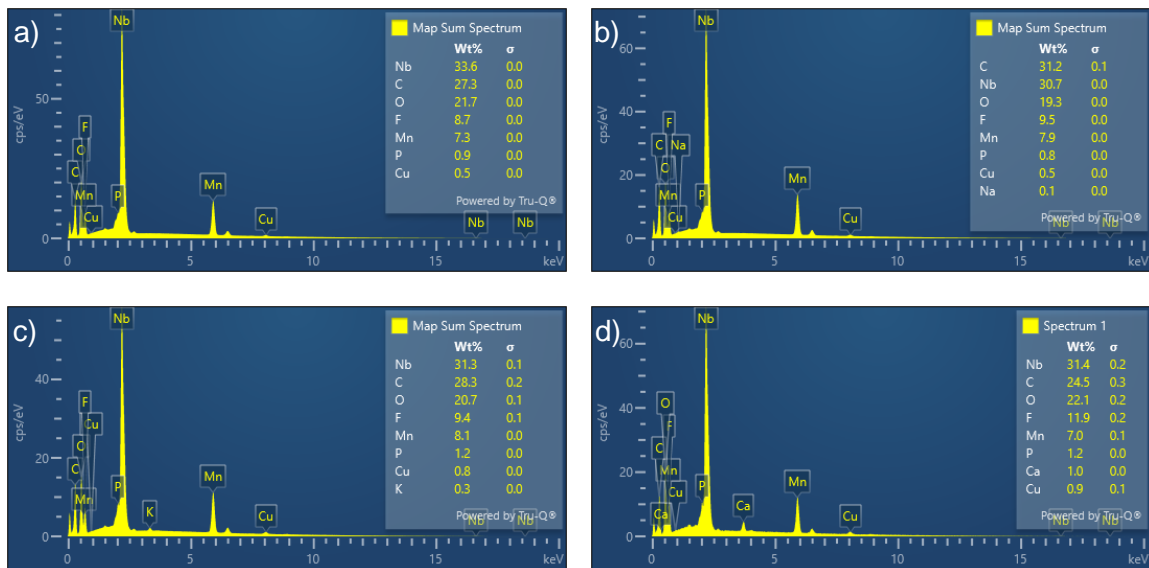


Figure S29: MnNb₂O₆ EDS spectra from electrodes after 1st cycle from a) Li, b) Na and c) K hydroxides, and d) Ca_{0.25}Mn_{0.75}Nb₂O₆. 20 kV, SE2 detector and working distance between 10–12 mm.

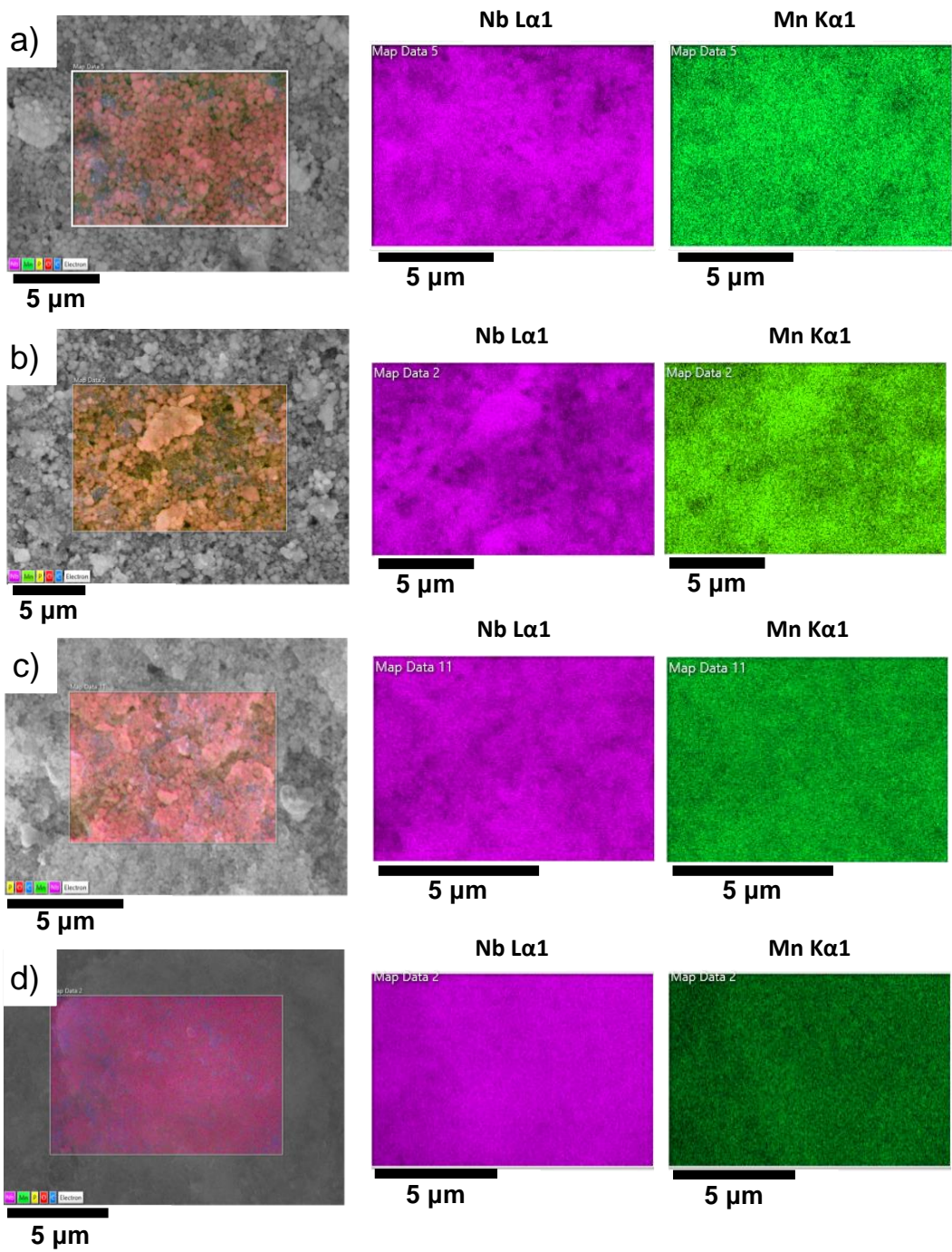


Figure S30: EDS elemental maps of MnNb_2O_6 from a) LiOH , b) NaOH , C) KOH , and d) $\text{Ca}_{0.25}\text{Mn}_{0.75}\text{Nb}_2\text{O}_6$. Nb La1 (pink), $\text{Mn K}\alpha 1$ (green).

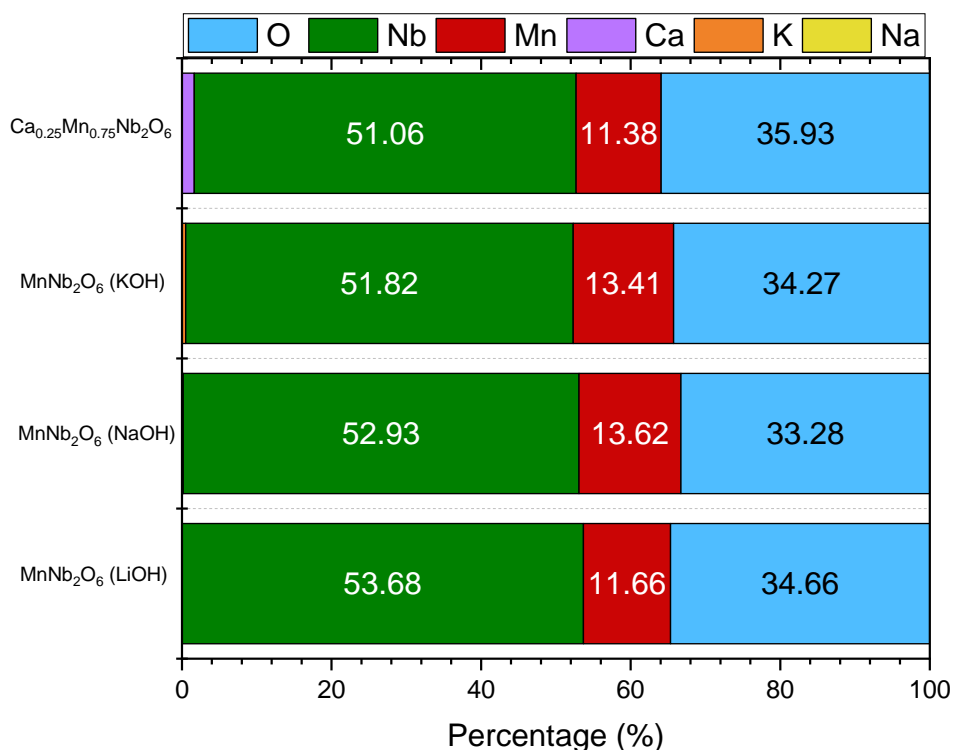


Figure S31: Calculated percentage of elements present in the electrodes after 1st cycle, using the EDS wt% for each element. Na and K percentages equal to 0.2 and 0.5%. The chemical formulae are $\text{Mn}_{0.73}\text{Nb}_2\text{O}_{5.73}$, $\text{Na}_{0.03}\text{Mn}_{0.87}\text{Nb}_2\text{O}_{5.88}$, $\text{K}_{0.05}\text{Mn}_{0.88}\text{Nb}_2\text{O}_{5.95}$, $\text{Ca}_{0.15}\text{Mn}_{0.75}\text{Nb}_2\text{O}_{5.90}$ by using metal ratios to calculate the oxygen stoichiometry.

Table S13. Comparison of the sample synthesised in this work and reported samples. Distinction is made by synthesis route, slurry composition, 1st charge specific capacity and cyclability.

Compositional space/ Synthesis method	Chemical Formula	Weight Ratio (AM:Carbon:Binder)/ Specific Capacity (1 st charge)	Specific Charge Capacity After Cycling
Mn ²⁺ -Nb ⁵⁺ -O without and anchored on graphene sheet ⁹ Hydrothermal synthesis (2 steps)	MnNb ₂ O ₆ MnNb ₂ O ₆ @rGO	8:1 (Super P):1 (PVDF) ~ 220 mA·h·g ⁻¹ ~ 460 mA·h·g ⁻¹ (0.05-3.0 V at 50 mA·g ⁻¹)	~ 80 mA·h·g ⁻¹ (0.05-3.0 V / 500 cycles) ~ 280 mA·h·g ⁻¹ (0.05-3.0 V / 500 cycles) 500 mA·g ⁻¹
Mn ²⁺ -Nb ⁵⁺ -O ^{8*} Hydrothermal synthesis (2 steps)	MnNb ₂ O ₆	7:1(acetylene back):1(PVDF) coated onto graphite sheet (Electrochemical testing in 1 M H ₂ SO ₄ solution) 350 F·g ⁻¹ (0.05-3.0 V at 1000 mA·g ⁻¹)	~ 320 F·g ⁻¹ (-0.1-1.1 V / 10000 cycles) 1000 mA·g ⁻¹
Mn ²⁺ -Nb ⁵⁺ -O ¹⁰ Hydrothermal synthesis (2 steps)	MnNb ₂ O ₆	7:2(acetylene back):1(PVDF) 308.3 mA·h·g ⁻¹ (0.01-3.0 V at 100 mA·g ⁻¹)	225 mA·h·g ⁻¹ (0.01-3.0 V / 400 cycles) 1000 mA·g ⁻¹
Mn ²⁺ -Nb ⁵⁺ -O ⁶ Solvothermal synthesis followed by annealing	MnNb ₂ O ₆	7:1.5 (Super P):1.5 (PVDF) 208 mA·h·g ⁻¹ (0.01-3.0 V at 38 mA·g ⁻¹)	352 mA·h·g ⁻¹ (0.01-3.0 V / 100 cycles) 38 mA·g ⁻¹
Mn ²⁺ -Nb ⁵⁺ -O ⁷ Electrospinning followed by annealing	Ultrathin amorphous C shells N doped-MnNb ₂ O _{6-x}	8:1(acetylene back):1(PVDF) -	~ 330 mA·h·g ⁻¹ (0.01-3.0 V / 2000 cycles) 100 mA·g ⁻¹
Mn ²⁺ -Nb ⁵⁺ -O	MNO-Li, MNO-Na, MNO-K	8:1 (C65):1 (PVDF) ~ 341, 256, 274 mA·h·g ⁻¹ (0.005-3.0 V at 10 mA·g ⁻¹)	~ 112, 182, 96 mA·h·g ⁻¹ (0.005-3.0 V / 200 cycles) at 200 mA·g ⁻¹

Hydrothermal synthesis (1 step) <i>This work</i>			
$\text{Ca}^{2+}\text{-Mn}^{2+}\text{-Nb}^{5+}\text{-O}$	CMNO	8:1 (C65):1 (PVDF)	$\sim 75 \text{ mA}\cdot\text{h}\cdot\text{g}^{-1}$ (0.005-3.0 V / 200 cycles) at $200 \text{ mA}\cdot\text{g}^{-1}$
Hydrothermal synthesis (1 step) <i>This work</i>		$\sim 201 \text{ mA}\cdot\text{h}\cdot\text{g}^{-1}$ (0.005-3.0 V at 10 $\text{mA}\cdot\text{g}^{-1}$)	

* Tested as a capacitor in an acidic aqueous electrolyte.

References

1. K. Momma and F. Izumi, VESTA 3 for three-dimensional visualization of crystal, volumetric and morphology data, *J. Appl. Crystallogr.*, 2011, **44**, 1272-1276.
2. B. M. Gatehouse, T. Negas and R. S. Roth, The crystal Structure of M-LiTa₃O₈ and its relationship to the mineral wodginite, *J. Solid State Chem.*, 1976, **18**, 1-7.
3. K. Kato, Structure refinement of H-Nb₂O₅, *Acta Crystallogr., Sect. B: Struct. Sci.*, 1976, **32**, 764-767.
4. H. Weitzel, Kristallstrukturverfeinerung von Wolframiten und Columbiten, *Z. Kristallogr. - Cryst. Mater.*, 1976, **144**, 238-258.
5. V. V. Atuchin, I. E. Kalabin, V. G. Kesler and N. V. Pervukhina, Nb 3d and O 1s core levels and chemical bonding in niobates, *J. Electron Spectrosc. Relat. Phenom.*, 2005, **142**, 129-134.
6. S.-Y. Lee, A. S. Lim, Y. M. Kwon, K. Y. Cho and S. Yoon, Copper, zinc, and manganese niobates (CuNb₂O₆, ZnNb₂O₆, and MnNb₂O₆): structural characteristics, Li⁺ storage properties, and working mechanisms, *Inorg. Chem. Front.*, 2020, **7**, 3176-3183.
7. Y. Lian, Y. Zheng, D. Wang, Y. Bai, H. Yan, Z. Wang, J. Zhao and H. Zhang, Ultrafast and stable ion/electron transport of MnNb₂O₆ in LIC/SC via interface protection and lattice defects, *J. Colloid and Interface Sci.*, 2022, **606**, 77-86.
8. T. Wang, T. F. Ma, T. Ge, S. J. Shi, H. M. Ji, W. L. Li and G. Yang, Synthesis of MnNb₂O₆ with hierarchical structure as a novel electrode material for high-performance supercapacitors, *J. Alloys Compd.*, 2018, **750**, 428-435.
9. X. Zhang, J. Zhang, S. Kong, K. Zhu, J. Yan, K. Ye, G. Wang, K. Cheng, L. Zhou and D. Cao, A novel calendula-like MnNb₂O₆ anchored on graphene sheet as high-performance intercalation pseudocapacitive anode for lithium-ion capacitors, *J. Mater. Chem. A*, 2019, **7**, 2855-2863.
10. T. Wang, T. Zhu, J. Wu, Z. Huang, Q. Chen, W. Hu, Y. Huang, S. Shi and W. Yin, The effect of hydrogen induced point defects on lithiation kinetics in manganese niobate anode, *J. Alloys Compd.*, 2021, **877**, 161090.